Mon. Not. R. Astron. Soc. **349,** 576–594 (2004) doi:10.1111/j.1365-2966.2004.07527.x

The Millennium Galaxy Catalogue: the photometric accuracy, completeness and contamination of the 2dFGRS and SDSS-EDR/DR1 data sets

N. J. G. Cross,[1⋆] S. P. Driver,[2] J. Liske,[3] D. J. Lemon,[4] J. A. Peacock,[5] S. Cole,[6] P. Norberg[7] and W. J. Sutherland[5]

[1]*Department of Physics and Astronomy, Johns Hopkins University, Baltimore, MD 21218, USA*
[2]*Research School of Astronomy and Astrophysics, The Australian National University, Weston Creek, ACT 2611, Australia*
[3]*ESO Headquarters Garching, Karl-Schwarzschild-Str. 2, D-85748 Garching bei München, Germany*
[4]*School of Physics and Astronomy, University of St Andrews, North Haugh, St Andrews, Fife KY16 9SS*
[5]*Institute for Astronomy, University of Edinburgh, Royal Observatory, Edinburgh EH9 3HJ*
[6]*Department of Physics, University of Durham, South Road, Durham DH1 3LE*
[7]*ETHZ Institut für Astronomie, HPF G3.1, ETH Hönggerberg, CH-8093 Zürich, Switzerland*

Accepted 2003 December 5. Received 2003 December 4; in original form 2003 May 29

ABSTRACT

The Millennium Galaxy Catalogue (MGC) is a deep ($\mu_{B,\rm lim} = 26$ mag arcsec^{-2}), wide-field, charge-coupled device imaging survey, covering 37.5 deg^2. The MGC survey region is completely contained within the Two-Degree Field Galaxy Redshift Survey (2dFGRS) and the Sloan Digital Sky Survey Early Data Release (SDSS-EDR). We compare the photometry and completeness of the 2dFGRS and the SDSS-EDR with the MGC over the range $16 < B < 20$ mag. We have also undertaken a photometric comparison to SuperCosmos (SCOS) and the Sloan Digital Sky Survey First Data Release (SDSS-DR1).

We find that $B_{\rm MGC} - B_{\rm 2dF} = (0.035 \pm 0.005)$ mag with an uncertainty of 0.142 mag per galaxy; $B_{\rm MGC} - B_{\rm SCOS} = (0.032 \pm 0.005)$ mag with an uncertainty of 0.108 mag; $B_{\rm MGC} - B_{\rm SDSS-EDR} = (0.032 \pm 0.005)$ mag with an uncertainty of 0.094 mag; and $B_{\rm MGC} - B_{\rm SDSS-DR1} = (0.039 \pm 0.005)$ mag with an uncertainty of 0.086 mag. We find that high surface brightness 2dFGRS galaxies are systematically too faint, which leads to a significant scale error in magnitude. This effect is significantly reduced with the SCOS photometry. In the SDSS there is a weak non-linear scale error, which is negligible for faint galaxies. Low surface brightness galaxies in the SDSS are systematically fainter, consistent with the relative shallowness of this survey.

We find that the 2dFGRS catalogue has (5.2 ± 0.3) per cent stellar contamination, (7.0 ± 0.4) per cent of objects resolved into two or more by the MGC, and is (8.7 ± 0.6) per cent incomplete compared to the MGC. From our all-object spectroscopic survey we find that the MGC is itself misclassifying (5.6 ± 1.3) per cent of galaxies as stars, and hence the 2dFGRS misses (14.3 ± 1.4) per cent of the galaxy population. The SDSS-EDR galaxy catalogue has (1.3 ± 0.1) per cent stellar contamination and (5.3 ± 1.0) per cent of galaxies misclassified as stars, with (0.18 ± 0.04) per cent of objects resolved into two or more by the MGC, and is (1.8 ± 0.1) per cent incomplete compared to the MGC. The total fraction of galaxies missing from the SDSS-EDR galaxy catalogue to $B_{\rm MGC} = 20$ mag, from incompleteness and misclassification, is (7.1 ± 1.0) per cent.

Key words: galaxies: general – cosmology: observations.

1 INTRODUCTION

Galaxy surveys are now becoming sufficiently extensive that eyeball verification of the entire automated detection and classification algorithms are impracticable. For example, the Two-Degree Field Galaxy Redshift Survey (2dFGRS) input catalogue (Colless et al. 2001, 2003) contains over 300 000 galaxies, for which redshifts have been targeted for 245 591 objects (229 118 galaxies, 16 348 stars and 125 quasars) and high-quality redshifts have been obtained for 221 414 galaxies. Numerous publications, based on this data set,

⋆E-mail: cross@pha.jhu.edu

© 2004 RAS

have been used to constrain cosmological parameters (e.g. Peacock et al. 2001; Efstathiou et al. 2002; Verde et al. 2002; Elgaroy et al. 2002) and to measure the local galaxy luminosity function(s) (see Folkes et al. 1999; Cole et al. 2001; Madgwick et al. 2002; Norberg et al. 2002b; de Propris et al. 2003), the bivariate brightness distribution (Cross et al. 2001; Cross & Driver 2002), star formation histories (Baldry et al. 2002; Lewis et al. 2002) and galaxy clustering (Norberg et al. 2001, 2002a), for example. The credibility of these papers relies, to some extent, upon the underlying accuracy and uniformity of the photometric input catalogue and its completeness [see, for example, Colless et al. (2001, 2003), Cross et al. (2001), Cole et al. (2001) and Norberg et al. (2002b), which each discuss various aspects of completeness, reliability and various selection biases].

Similarly the Sloan Digital Sky Survey (SDSS),[1] which will eventually provide photometric information for over one billion objects (York et al. 2000), will also be publicly released in stages (e.g. Stoughton et al. 2002), and the value to the community will depend upon the accuracy of the automated photometric, astrometric and object classification algorithms (see, for example, Yasuda et al. 2001; Blanton et al. 2003). Here we aim to provide an independent estimate of the photometric and classification credibility of these public data sets, through the comparison with a third, manually verified, data set, namely the Millennium Galaxy Catalogue (MGC; Liske et al. 2003; Lemon 2003).[2]

The MGC is particularly suitable as it covers a sufficiently large area ($\sim$37.5 deg^2) to ensure statistically significant overlap in terms of object numbers, yet is sufficiently small for all objects ($B_{\rm MGC} < 20$ mag) to have been manually inspected (for all non-stellar objects) and corrected, providing a robust and reliable survey. The MGC also probes to a substantially deeper isophote ($\mu_{B,\rm lim} = 26$ mag arcsec^{-2}; Liske et al. 2003) than either the original Automated Plate Measuring machine (APM) plate scans (upon which the 2dFGRS input catalogue is based) or the SDSS drift scans (both with $\mu_{B,\rm lim} \approx 24.5$ mag arcsec^{-2}; Maddox et al. 1990a; York et al. 2000). The resulting higher signal-to-noise ratio allows more reliable photometric measurement, object classification and (de)blending fixes. The deeper isophote also allows a fully independent assessment of the completeness with regard to low surface brightness galaxies (LSBGs; see Impey & Bothun 1997). Likewise the higher resolution and better mean seeing allow an assessment of the completeness for high surface brightness galaxies (HSBGs; see e.g. Drinkwater 1999). These latter concerns are aired in detail in (Sprayberry et al. 1997 see also O'Neil & Bothun 2000) who, following on from Disney (1976), argue for incompleteness levels of as much as 50 per cent in nearby galaxy catalogues such as the APM. If this is indeed correct, then a deeper survey such as the Millennium Galaxy Catalogue should uncover a significant number of galaxies either missed or with fluxes severely underestimated by the shallower surveys.

In this paper we describe the three independent imaging surveys (MGC, 2dFGRS and SDSS Early Data Release) and the catalogue matching process in Sections 2 and 3. We quantify the photometric accuracy as a function of magnitude and surface brightness in Section 4, including recent updates to the 2dFGRS including SuperCosmos (SCOS) data and the recently released SDSS First Data Release, and we quantify the reliability of the star–galaxy separation in Section 5. Finally we explore the crucial question of completeness across the apparent magnitude–apparent surface brightness plane (M–Σ) in Section 6. We summarize our findings in Section 7.

2 DATA

Here we briefly introduce the three imaging catalogues that we wish to compare: the Millennium Galaxy Catalogue (MGC; Liske et al. 2003), the Two-Degree Field Galaxy Redshift Survey (2dFGRS; Colless et al. 2001, 2003), and the Sloan Digital Sky Survey (SDSS; Stoughton et al. 2002; Abazajian et al. 2003). The MGC is adopted as the yardstick against which we shall quantify the photometric accuracy, completeness and contamination of the 2dFGRS and SDSS Early Data Release (EDR) and First Data Release (DR1) data sets. This is for a number of reasons:

(i) The internal accuracy of the MGC photometry is shown to be $\pm$0.023 mag, for stars and galaxies over the magnitude range 16–21. This is superior to the quoted accuracies of the 2dFGRS and SDSS-EDR data sets ($\pm$0.15 mag, Norberg et al. 2002b, and $\pm$0.033 mag, Stoughton et al. 2002, respectively).

(ii) The MGC is the deepest, in terms of sky noise, of the three surveys, extending to $\mu_{B_{\rm MGC,lim}} = 26.0$ mag arcsec^{-2} (cf. $\mu^{\rm 2dFGRS}_{b_{\rm J,lim}} = 24.67$ mag arcsec^{-2}, Pimbblet et al. 2001, and $\mu^{\rm SDSS\text{-}EDR}_{g^*,\rm lim} = 24.3$ mag arcsec^{-2}, Stoughton et al. 2002).

(iii) The MGC uses a fixed isophotal detection limit ensuring uniform survey completeness.

(iv) The MGC has the best median seeing of the three surveys with full width at half-maximum $\langle {\rm FWHM_{MGC}} \rangle = 1.3$ arcsec (compared to $\langle {\rm FWHM_{2dFGRS}} \rangle \sim 2.5$ arcsec and $\langle {\rm FWHM_{SDSS-}}_{EDR} \rangle \sim 1.6$ arcsec).

(v) All galaxies in the MGC to $B_{\rm MGC} = 20$ mag have been verified by eye and where necessary corrected for classification errors (overblending, underblending).

(vi) All charge-coupled devices (CCDs) have been carefully inspected and artefacts masked out (including satellite trails, hot pixels, bad columns and diffraction spikes). Bright stars (on and off the image) and bright galaxies have also been masked out, and asteroids and cosmic rays have been carefully identified (see Liske et al. 2003).

Fig. 1 shows the region of overlap between the three surveys resulting in a $\sim$30 deg^2 region in common comprising $\sim$10 000 MGC galaxies in the magnitude range $16 < B_{\rm MGC} < 20.0$ mag (see Table 1).

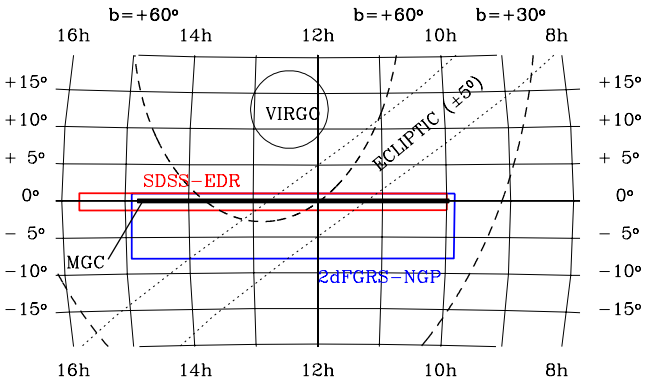

Figure 1. A section of an Aitoff projection showing the overlap between the three surveys covered in this paper. Also shown are contours of constant Galactic latitude (dashed lines), the location of the ecliptic and the Virgo cluster.

[1] The SDSS website is http://www.sdss.org/

[2] The Millennium Galaxy Catalogue is a publicly available data set found at http://www.eso.org/~jliske/mgc/ or by request to jliske@eso.org (see Liske et al. 2003).

2.1 Millennium Galaxy Catalogue

The Millennium Galaxy Catalogue (Liske et al. 2003, henceforth MGC1) is a deep $\sim$37.5 deg^2 B-band CCD imaging survey. It spans the equatorial strip from $9^h58^m28^s$ to $14^h46^m45^s$ with a declination range from $-0^\circ17'\,15''$ to $+0^\circ17'\,15''$ (J2000.0). The imaging was carried out using the four-CCD mosaic Wide Field Camera on the Isaac Newton Telescope between 1999 March and 2000 April and consists of 144 overlapping pointings. The data were taken during dark time with a median seeing FWHM = 1.3 arcsec, with pixel size 0.333 arcsec; all objects are therefore fully sampled. Full details of the data collection, photometric and astrometric solutions along with the image detection, analysis and eyeball classifications are given in MGC1 and summarized briefly below.

Objects were detected using Source Extractor (SExtractor, Bertin & Arnouts 1996) with a fixed isophotal detection threshold of $\mu_{B_{\rm MGC,lim}} = 26$ mag arcsec^{-2}. The final MGC magnitudes are dust-corrected (Schlegel, Finkbeiner & Davis 1998) SExtractor 'best' magnitudes, which are derived from an elliptical aperture of 2.5 Kron radii (Kron 1980), unless the nearby neighbour flag is set, in which case the Gaussian-corrected isophotal magnitude is used. From the overlap regions between adjacent pointings we have determined that the internal astrometric and photometric error distributions are well described by Gaussians of FWHM $\pm$0.08 arcsec and $\pm$0.023 mag respectively (see figs 5 and 7 of MGC1). The calibration solution from Landolt standards indicates that the absolute zero-point is accurate to $\pm$0.005 mag.

The MGC was separated into two magnitude ranges, forming the MGC-BRIGHT ($16.0 < B_{\rm MGC} < 20.0$ mag) and MGC-FAINT ($20.0 \leqslant B_{\rm MGC} < 24.0$ mag) catalogues. For the purposes of this paper we now focus on MGC-BRIGHT. We note that the stellarICITY distribution is extremely bimodal, indicating reliable star–galaxy separation (see fig. 9 of MGC1). Even so, all objects with stellarICITY < 0.98 were visually inspected, classified and, where necessary, repaired manually for erroneous deblending, erroneous background estimation or contamination from nearby objects. A flag was assigned for each galaxy indicating whether its photometry was considered 'good', 'compromised' or 'corrupted'.

Bright stars, diffraction spikes, bad columns, hot pixels, satellite trails, bad charge transfer regions and CCD edges were masked. Objects within a 50-pixel threshold of a masked pixel were removed from the catalogue to produce a final pristine fully eyeball-verified catalogue of 9795 galaxies (9657 'good', 137 'compromised' and 0 'corrupted') within a reduced survey area of 30.90 deg^2 over the magnitude range $16 < B_{\rm MGC} < 20$ mag.

Half-light radii were measured for all galaxies within MGC-BRIGHT and are equal to the semimajor axis of the ellipse that contains half of the flux of the galaxy. The effective surface brightness is then derived assuming a circular aperture [i.e. $\mu_{\rm eff} = B_{\rm MGC} + 2.5\log_{10}(2\,\pi\,r_{\rm hlr}^2)$]. If the galaxy is an inclined optically thin disc galaxy, this will correct the effective surface brightness to the face-on values [see Cross & Driver (2002) for a more detailed discussion of the implications of this].

2.2 Two-Degree Field Galaxy Redshift Survey

The 2dFGRS contains both photometric and spectroscopic data for 229 118 galaxies selected from the Automated Plate Measuring machine (APM) galaxy catalogue (Maddox et al. 1990a,b). The 2dFGRS target catalogue covers 2152 deg^2 to a limiting magnitude of $b_{\rm j,old} = 19.45$ mag, where $b_{\rm j,old}$ is the photometry of the galaxies at the beginning of the 2dFGRS campaign, before photometry updates in 2001 and 2003.

We will briefly describe the calibration process here, but the full calibration and recalibration up to and including the 2001 recalibration is described in detail in Maddox et al. (1990a) and Norberg et al. (2002b).

The APM images come from photographic plates collected on the UK Schmidt Telescope (UKST) 20 to 30 yr ago and digitized by the APM team. The APM magnitudes were measured with an approximate surface brightness limit of $\mu_{b_{\rm j,lim}} \sim 24.67$ mag arcsec^{-2} (see Cross et al. 2001; Pimbblet et al. 2001). The original isophotal magnitudes were adjusted assuming a Gaussian profile to produce pseudo-total magnitudes (see Maddox et al. 1990b for details). For a subsample total CCD magnitudes were obtained and converted to the $b_{\rm j}$ band using $b_{\rm j} = B - 0.28(B - V)$ (Blair & Gilmore 1982). A calibration curve was determined by minimizing the residuals between the APM $b_{\rm j}$ and the CCD $b_{\rm j}$.

When the 2dFGRS target catalogue was determined, in 1994, more CCD data were available (see Norberg et al. 2002b). New offsets between the original field-corrected total magnitudes and the final magnitudes were obtained, assuming a fixed scale of 1, to select the sample. While any scale error will produce errors in the bright magnitudes, it will not affect the selection of targets at $b_{\rm j} = 19.45$. Additional UKST plates outside the APM Galaxy Survey were reduced using the standard APM galaxy survey procedures to improve the efficiency of the 2dFGRS observing strategy. These additional fields contained data in the region $9^h < {\rm RA} < 15^h$ and $-7\fdg5 < {\rm Dec.} < 3\fdg5$ (J2000.0). These additional data were calibrated separately using CCD data from Raychaudhury et al. (1994) and contain the data used in this paper. The magnitudes were then dust-corrected using the dust maps supplied by David Schlegel, similar to the maps in Schlegel et al. (1998).

In 2001, the subset of the APM representing the 2dFGRS input catalogue was recalibrated further using European Imaging Survey Data (Arnouts et al. 2001) to provide an absolute revised zero-point for plate number UKST 411. The $(b_{\rm j} - J)$ colour versus $b_{\rm j}$ relation was then derived for UKST 411 using J-band data from the Two-Micron All Sky Survey (2MASS, Jarrett et al. 2000). However, this revision does not affect the target selection in the 2dFGRS, and it is not relevant to this paper.

In 2003 April, the photometry was recalibrated once again by comparing magnitudes calculated from APM scans with magnitudes calculated from SuperCosmos (SCOS, Hambly et al. 2001) scans (see Colless et al. 2003; Peacock et al., in preparation, for details). The SCOS data were calibrated from external CCD sources (mainly SDSS-EDR with updated zero-points), but with the mean 2MASS $(b_{\rm j} - J)$ on each plate forced to be the same. The UKST $b_{\rm j}$ and $r_{\rm f}$ plates were calibrated separately, but then a final iteration was performed to keep the distribution of $b_{\rm j} - r_{\rm f}$ colours uniform. Finally the original APM data were regressed to fit the SuperCosmos data for each plate. The absolute precision of the photometry is limited by the uniformity of the 2MASS photometry, which is claimed to be good to 0.03 mag over the whole sky.

The SCOS data include both $b_{\rm j}$ and $r_{\rm f}$ magnitudes from the same plates as the APM data, but with independent scanning and calibration. These are included in the main 2dFGRS data base (see Colless et al. 2003). In Section 4 we test the photometry of SCOS as well as 2dFGRS against the MGC.

The final dust-corrected 2dFGRS $b_{\rm j}$ magnitudes will be referred to as $b_{\rm 2dF}$ throughout. Since the 2dFGRS selection limit was $b_{\rm 2dF,old} = 19.45$ mag, the redshift survey does not have a fixed limiting magnitude. The SCOS $b_{\rm j}$ and $r_{\rm f}$ magnitudes will be referred to as $b_{\rm SCOS}$ and $r_{\rm SCOS}$.

Star–galaxy separation was implemented as described in Maddox et al. (1990a). They estimate that the star classification is reliable with ∼5 per cent stellar contamination to a limit of $b_{2dF,old} \approx 20.4$ mag.

2.3 Sloan Digital Sky Survey

We use data from the SDSS Early Data Release (SDSS-EDR) and SDSS First Data Release (SDSS-DR1). The SDSS-EDR (Stoughton et al. 2002) consists of eight drift scan stripes covering three regions obtained via a dedicated 2.5-m telescope at the Apache Point Observatory. The 2001 EDR region covers a total of 462 deg^2 providing photometry in u^*, g^*, r^*, i^* and z^* for ∼14 million objects to approximate point source detection limits of 22.0, 22.2, 22.2, 21.3 and 20.5 mag respectively. The SDSS-DR1 (Abazajian et al. 2003) covers 2099 deg^2, in u, g, r, i and z including the SDSS-EDR, with improvements to the data extraction. While these improvements include deblending, astrometry and spectroscopy, the main improvements are in the photometry. Since most of the deblending problems are for $r < 15$ galaxies, this will not significantly affect our completeness. Therefore we have stuck to the SDSS-EDR in the completeness and contamination sections.

The effective integration time of SDSS is 54 s, yielding an approximate isophotal detection limit of $\mu_{g^*,lim} = 24.3$ mag arcsec^{-2} and $\mu_{r^*,lim} = 24.1$ mag arcsec^{-2}. The data overlapping the MGC and 2dFGRS (stripes 752 and 756) were taken through variable conditions, with seeing ranging from 1.0 to 3.0 arcsec (see fig. 8 of Stoughton et al. 2002). Photometric calibration is made with the use of a nearby telescope to measure nightly extinction values and 'observation transfer fields' which lie within the SDSS survey areas.

Image detection, analysis and classification were undertaken using in-house automated software, producing a final set of 120 parameters or flags per object. Full details of the data reduction pipeline are given in Stoughton et al. (2002) and references therein. Preliminary galaxy number counts and discussion of the completeness and contamination at magnitudes brighter than $g^* = 16$ mag are given in Yasuda et al. (2001).

The final SDSS data base defines a number of magnitude measurements and we shall adopt the reddening-corrected Petrosian magnitudes (see Fukugita et al. 1996) as closest to total – shown to have no surface brightness dependence for a well-defined profile shape. The final quoted SDSS-EDR photometric accuracy is ±0.033 mag and the pixel size is 0.396 arcsec.

In the SDSS literature, there are many methods of star–galaxy classification. We have taken the classifications used in the SDSS-EDR data base, which are calculated as prescribed in Stoughton et al. (2002). They separate stars from galaxies using the difference between the point spread function (PSF) and model magnitude in r^*. Galaxy target selection requires a difference greater than 0.3 mag.

2.4 Additional redshift data

The redshift data from 2dFGRS and SDSS-EDR have also been supplemented with 6065 additional redshifts taken by the authors using the 2dF instrument. These are the first part of a data set designed to provide a complete sample of galaxies with $B_{MGC} < 20.0$ mag, selected from the MGC, and a complete sample of stars with $B_{MGC} < 20.0$ mag for a section of the survey. We have also added in 4007 redshifts from the NASA Extragalactic Database (NED), 736 redshifts from the 2dF QSO Redshift Survey (2QZ), 55 redshifts from Paul Francis' Quasar Survey (Francis, Nelson & Cutri 2004) and 11 LSBG redshifts (Impey et al. 1996). There are many galaxies for which we have multiple redshifts and we have a high overall completeness. Out of the 9795 ($16 < B_{MGC} < 20$ mag) MGC objects classified as galaxies, 8837 have redshifts, 90.2 per cent. This proportion rises to 96.0 per cent for $16 < B_{MGC} < 19.5$ mag galaxies and 98.8 per cent for $16 < B_{MGC} < 19$ mag galaxies. There are also 2907 MGC stellar-like objects ($16 < B_{MGC} < 20$ mag) with measured velocities.

2.5 Filter conversions

We elect to work in the B_{MGC} band, for which the following filter conversions have been derived – based upon Fukugita et al. (1996), Norberg et al. (2002b), Smith et al. (2002) and MGC1. The full details of this analysis are found in the Appendix. The four colour equations are for 2dFGRS, SCOS, SDSS-EDR and SDSS-DR1 respectively:

$$B_{MGC} = b_{2dF} + 0.121(g^* - r^*) - 0.012, \quad (1)$$

$$B_{MGC} = b_{SCOS} + 0.108(b_{SCOS} - r_{SCOS}) - 0.044, \quad (2)$$

$$B_{MGC} = g^* + 0.251(g^* - r^*) + 0.178, \quad (3)$$

$$B_{MGC} = g + 0.251(g - r) + 0.178. \quad (4)$$

We use the colours from each data set where possible. For the 2dFGRS we use the SDSS-EDR colours, since much of the 2dFGRS calibration was done using the SDSS-EDR. We also tried using the SCOS r_f data for the 2dFGRS colour equation. This gave similar photometric results when compared to other surveys, but with more scatter.

2.6 Masking and areal coverage

All three surveys contain unobserved regions due to a variety of issues, most notably bright stars (2dFGRS), failed scans (SDSS-EDR) and CCD cracks/boundaries (MGC). As the MGC is wholly contained within the 2dFGRS and SDSS-EDR regions we trim all three catalogues to an approximate 44 deg^2 common range defined by the MGC: $9^h58^m00^s < \alpha_{J2000} < 14^h47^m00^s$ and $-00^\circ18'\,00'' < \delta_{J2000} < 00^\circ18'\,36''$. Within this rectangle the MGC covers 37.5 deg^2, of which 30.9 deg^2 is considered high quality. The SDSS-EDR contains three holes within this region, and the 2dFGRS contains a number of star 'drill'-holes. Taking all exclusion regions into account, we are left with a final high-quality fully covered common area of 29.74 deg^2. The number of objects contained within this common region for each of the three surveys is shown in Table 1. Fig. 2 shows the common region with the individual masks overlaid for the MGC (light grey), 2dFGRS (dark grey) and SDSS-EDR (black) surveys respectively.

3 CATALOGUE MATCHING

3.1 Matching MGC to 2dFGRS

The catalogue of 2dFGRS objects described in Section 2.2 was matched to the {MGC-BRIGHT} catalogue ($B_{MGC} < 20.0$ mag) by finding the nearest match within a radius of 5 arcsec. Various radii were tested (see Fig. 3). While the minimum sum of the non-matches and multiple matches is 4 arcsec, most close-in multiple matches

Table 1. Summary of objects and depth within the common area for the three surveys.

Survey	Range (mag)	No. gals	No. stars
MGC-BRIGHT	$16.0 < B_{\rm MGC} < 20.0$	9795	36 260
SDSS-EDR	$16.0 < B_{\rm MGC} < 20.0$	10 213	34 779
2dFGRS	$16.0 < B_{\rm MGC} < 19.5$	5215	–
MGC-BRIGHT	$16.0 < B_{\rm MGC} < 19.5$	5792	28 271
SDSS-EDR	$16.0 < B_{\rm MGC} < 19.5$	6063	27 026

occur when a 2dFGRS object is composed of two or more MGC matches (see Cross 2002 for more details) rather than a nearby unassociated object being wrongly matched. The gradient of the number of multiple objects reaches a maximum at 5 arcsec, indicating that most multiples are due to poor resolution within this radius. Thus 5 arcsec gives the optimal radius to maximize the number of real matches.

Each 2dFGRS object was also checked for multiple matches within an ellipse defined by its isophotal area, eccentricity and orientation. If an MGC object contributes to the flux of the 2dFGRS object, its centre should lie within the area of the 2dFGRS object. To find multiple and faint matches, objects in {MGC-FAINT} with $B_{\rm MGC} < 21.0$ mag were also matched. The edge s of the 2dFGRS object is defined as

$$s = \{[\cos(\theta)/a]^2 + [\sin(\theta)/b]^2\}^{-1/2}, \quad (5)$$

where a is the length of the semimajor axis, b is the length of the semiminor axis and θ is the bearing from the 2dFGRS object to the MGC object and the orientation of the 2dFGRS object on the sky. Lengths a and b are defined from the area (A) and the eccentricity (e):

$$a = \sqrt{(A/\pi)}(1 - e^2)^{-0.25}, \quad (6)$$

$$b = \sqrt{(A/\pi)}(1 - e^2)^{0.25}. \quad (7)$$

If the MGC object lies at $r \leqslant s$ then it is a component of the 2dFGRS object. The main component is deemed to be the brightest, unless the redshift is incompatible with the MGC star–galaxy

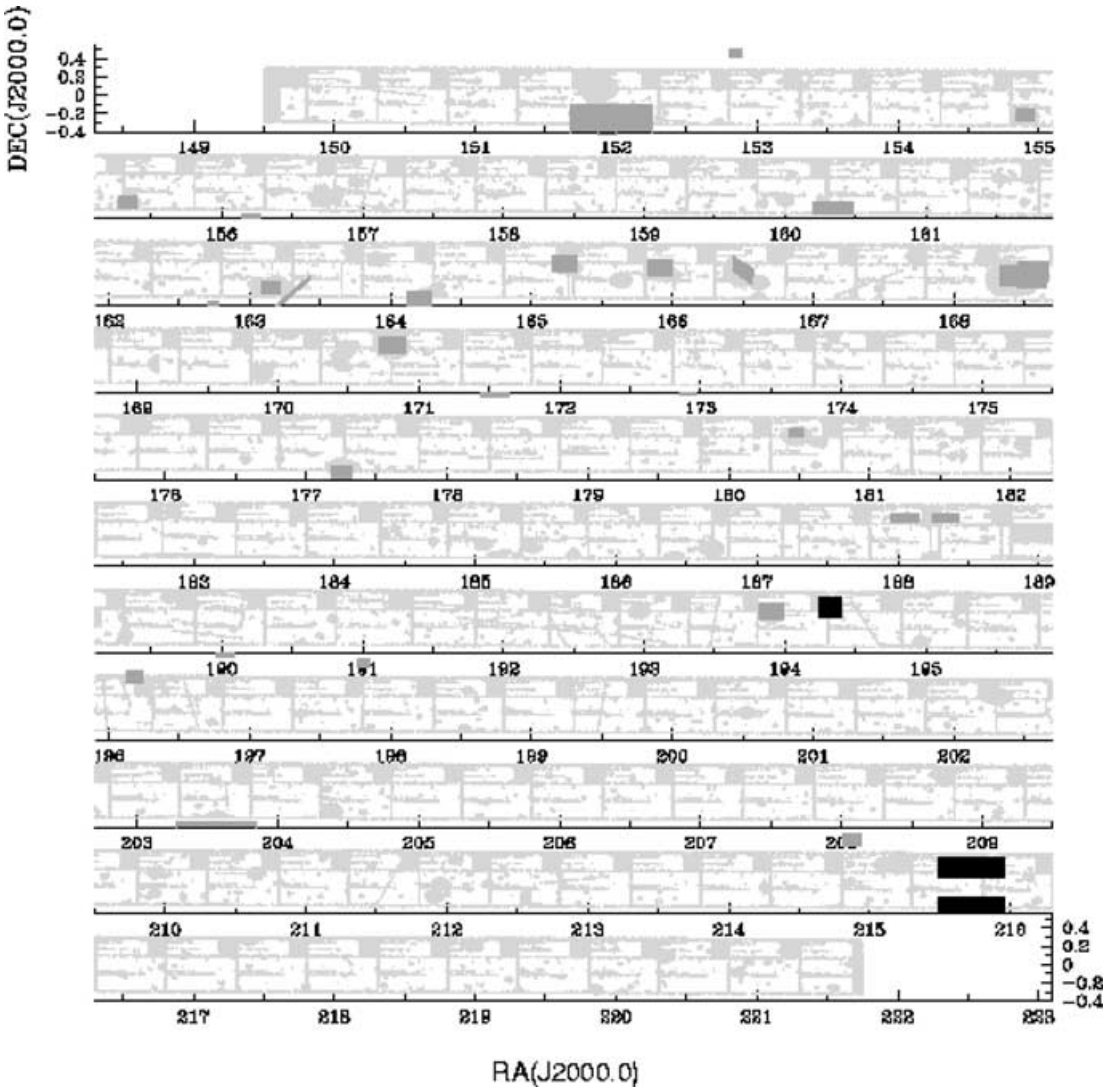

Figure 2. The common region for the three surveys. The light grey, dark grey and black regions represent exclusion regions from the MGC, 2dFGRS and SDSS-EDR, respectively. The remaining white area covers 29.74 deg^2 and represents the region in common between the three imaging surveys.

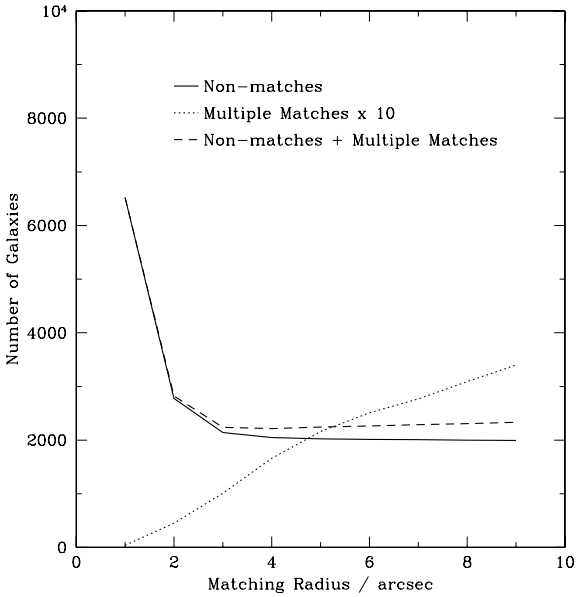

Figure 3. The solid line shows the number of 2dFGRS galaxies *not* matched to MGC galaxies. The dotted line shows the number of multiple matches multiplied by 10, and the dashed line shows the sum of the non-matches and multiple matches.

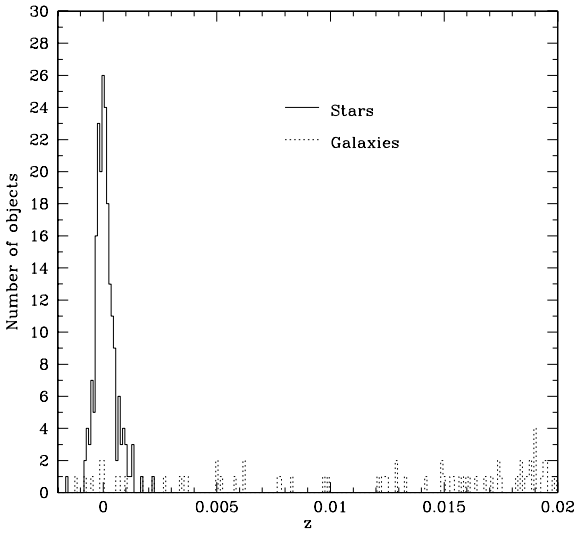

Figure 4. Histograms of the redshift distributions of stars (solid line) and galaxies (dotted line) of 2dFGRS objects at low redshift. Stars have a narrow distribution with width $\sim 1.0 \times 10^{-3}$ centred on $z = 0$.

classification. Using both methods allows for some error in the position and picks up almost all the matches first time. A few (five) matches were missed by both methods, because they were slightly too wide or slightly too faint. These were put in later by hand. Fig. 4 shows single-component MGC–2dFGRS matches at $z < 0.02$. The solid histogram shows the objects that are classified as stars in the MGC and the dotted histogram shows the objects that are classified as galaxies in the MGC. It is clear that the stellar population has a distribution with $z \leqslant 2.0 \times 10^{-3}$, at which redshift there are very few galaxies. For multiple matches the MGC comparison magnitude is taken as the sum of all components lying within the 2dFGRS object's isophotal area. All failed matches were checked by eye. Many were objects lying close to the exclusion boundaries. The 2dFGRS contains 5346 objects within the common region ($B_{\rm MGC} > 16.0$ mag), of which matches are found for 5285 and 61 have no matches. Of these mismatches eight are due to the MGC objects lying across an exclusion boundary (close to bright stars) and 53 are genuine mismatches. Four of these are due to over-deblending of very bright galaxies by the APM process and 49 have no obvious counterparts on the MGC data and must represent plate artefacts, asteroids, satellite trails, diffraction spikes or other such objects. These are described in Section 5.2.

The 2dFGRS–MGC catalogue was then inverted so that the MGC was the reference catalogue. If the MGC object had $B_{\rm MGC} \geqslant 20$ mag, it was removed. All additional components from the matching done above, with $B_{\rm MGC} < 20$ mag, were also added in. Finally each MGC galaxy was checked for multiple 2dFGRS objects within an ellipse defined by the MGC ellipticity, isophotal area and position angle. There are 46 364 MGC objects in the common region, of which 9795 are classified as galaxies, 36 260 are classified as stars, and 309 are classified as asteroids, cosmic rays, noise detections or obsolete (see Liske et al. 2003). Of the 9795 galaxies, 4646 have a single match to 2dFGRS galaxies, 405 have two or more MGC objects (of which the brightest is a galaxy) matched to one 2dFGRS objects, 2 have two or more 2dFGRS objects matched to one MGC galaxy, and 4742 have no match, mainly because the MGC limiting magnitude is fainter than the 2dFGRS limits.

3.2 Matching the SDSS-EDR to the MGC

A similar strategy to the above was employed for the matching of the MGC and SDSS-EDR catalogues. The only exception was in the handling of multiple matches, where the MGC data could not be guaranteed to have superior resolution in all cases. Hence for multiple matches we also employ a nearest-neighbour routine. This produces a match if and only if galaxy A is the nearest object to galaxy B and galaxy B is the nearest object to galaxy A. It also identifies secondary components as objects where a second galaxy C has A as the nearest match. For each galaxy we find the neighbours using both methods. The components of a particular galaxy are those selected by both routines. There are 44 992 SDSS objects $[16 < g^* + 0.251(g^* - r^*) + 0.178 < 20$ mag] in the common region, of which 10 213 are classified as galaxies and 34 779 are classified as stars. Of the 10 213 galaxies, 9039 have clear matches to MGC galaxies, 18 have multiple matches to MGC objects (of which the brightest is a galaxy), 260 have matches to star-like MGC objects, and 858 have no match. Of the 34 779 stars, 34 213 have matches to single MGC stars, 35 have multiple matches, with the brightest matching to a star, 9 are matched to non-stellar objects, and 521 have no match. After comparison to {MGC-FAINT}, the non-matches reduced to 329 galaxies and 335 stars. These are discussed in Section 5.2.

4 PHOTOMETRIC COMPARISON

All the following numbers are selected with $16 < B_{\rm MGC} < 20$ mag to avoid problems with saturation at the bright end. After matching to the MGC we find unambiguous single–single object matches in the common region for 4418 2dFGRS objects and 44 690 SDSS-EDR objects and a further 589 (11.7 per cent) and 893 (2.0 per cent) ambiguous or multiple matches respectively. The ambiguous matches are MGC galaxies matched to 2dFGRS/SDSS-EDR stars

Table 2. Summary of the relative photometry of galaxies. This table lists the offset, average standard deviation per galaxy and the parameters a and b from equation (12). We list each set of numbers for the full range of magnitudes, for the three-way cross-check ($16 < B_{\rm MGC} < 19$ and for the faint sample $19 < B_{\rm MGC} < 20$.

Data	Full range of data					Best sample $16 < B < 19$				Faint sample $19 < B < 20$			
	Mean	σ	a	b	χ^2_ν	Mean	a	b	χ^2_ν	Mean	a	b	χ^2_ν
MGC–2dF	0.035	0.142	0.114	0.057	1.28	0.012	0.099	0.051	1.45	–	–	–	–
MGC–SCOS	0.032	0.108	0.096	0.045	3.28	0.017	0.093	0.044	4.39	–	–	–	–
MGC–EDR	0.032	0.094	0.045	0.014	9.72	0.026	0.073	0.026	3.33	0.036	0.036	−0.002	1.03
MGC–DR1	0.039	0.086	0.051	0.013	14.0	0.034	0.082	0.027	5.06	0.042	0.040	−0.006	1.01
2dF–DR1	0.004	0.151	−0.044	−0.037	1.14	0.019	−0.029	−0.028	0.60	–	–	–	–
SCOS–DR1	0.005	0.104	−0.024	−0.021	0.87	0.013	−0.017	−0.018	0.69	–	–	–	–
DR1–EDR	−0.007	0.037	−0.008	−0.000	1.98	−0.008	−0.011	−0.002	1.41	−0.007	−0.007	0.000	1.53
SCOS–EDR	−0.002	0.107	−0.035	−0.023	0.75	0.006	−0.031	−0.021	0.79	–	–	–	–
2dF–EDR	−0.003	0.154	−0.052	−0.037	1.04	0.011	−0.038	−0.029	0.59	–	–	–	–
SCOS–2dF	0.001	0.086	0.018	0.012	1.71	−0.006	0.009	0.009	0.93	–	–	–	–

Table 3. Summary of the relative photometry between stellar objects. The columns listed give the mean, standard deviation per star, scale error (see equation 12) and the aperture-corrected mean and standard deviation corrected for field-to-field variation.

Data	Mean	σ	a	b	χ^2_ν	Best mean[a]	Best σ[b]
MGC–EDR	−0.031	0.057	−0.038	−0.004	96.6	0.035	0.046
MGC–DR1	−0.022	0.057	−0.028	−0.004	90.3	0.044	0.046

[a]The best mean has aperture corrections removed. There is a 0.066 mag correction for Petrosian to Kron magnitudes.
[b]The best σ has field-to-field variations removed.

or vice versa. For the purposes of photometric comparisons we now consider only the unambiguous single–single object matches. However, first it is worth considering the various magnitudes used in this section. The MGC adopts Kron magnitudes (Kron 1980) defined by an elliptical aperture of major axis 2.5 Kron radii and ellipticity as defined by the initial SExtractor parameters. The 2dFGRS uses isophotally corrected magnitudes with subsequent corrections for zero-point offsets and scale errors (see Norberg et al. 2002b). The SDSS-EDR uses Petrosian magnitudes (see Blanton et al. 2001). All magnitude systems have their virtues and failings, and we defer a prolonged discussion of this by simply choosing to compare the final quoted magnitudes for each survey as seen by the user. As a reminder we note that Petrosian magnitudes are known to underestimate the total magnitudes for Gaussian, exponential and de Vaucouleurs profiles by 0.07, 0.01 and 0.22 mag respectively, whereas Kron magnitudes are known to underestimate the same profiles by 0.01, 0.04 and 0.10 mag respectively (see Cross 2002). The 2dFGRS isophotally corrected magnitudes are deemed total and no quantifiable error for profile shapes is known.

Hence our comparison will naturally incorporate discrepancies in photometry, methodology and spectral shape assumptions in the colour conversions resulting in a 'real-life' assessment of the error budget. While the dust correction is part of the 'real-life' assessment, it varies as a function of position, and so must be dealt with separately. Therefore we do the photometry on magnitudes uncorrected for extinction throughout.

The extra dust correction terms are important since all the magnitudes have been dust-corrected independently, albeit based upon the same dust maps (Schlegel et al. 1998). It was found that the different values of $A/E(B-V)$ were slightly inconsistent and contributed the following additional offsets to the data:

$$\Delta B^{\rm DC}({\rm MGC–2dFGRS}) = -0.002, \quad (8)$$

$$\Delta B^{\rm DC}({\rm MGC–SDSS}) = -0.007, \quad (9)$$

$$\Delta B^{\rm DC}({\rm 2dFGRS–SDSS}) = -0.005. \quad (10)$$

The corrections for 2dFGRS and SCOS are the same and the corrections for the SDSS-EDR and SDSS-DR1 are the same. The dust corrections do not appear to increase the variance. This additional offset is directly proportional to the mean dust correction over the survey strip, $\overline{E(B-V)} = 0.033 \pm 0.010$. The additional offsets can be calculated in other parts of the sky using the following equation:

$$\Delta B^{\rm DC} = \Delta[A/E(B-V)]\overline{E(B-V)}, \quad (11)$$

where $\Delta[A/E(B-V)] = 0.06$, 0.21 and 0.15 for MGC–2dFGRS, MGC–SDSS and 2dFGRS–SDSS respectively. The SCOS and SDSS-DR1 photometry is added to the 2dFGRS and SDSS-EDR matches respectively. The full summary of all the cross-checks is given in Tables 2, 3 and 4, which list galaxy scale errors, stellar photometry and errors with surface brightness respectively.

4.1 Magnitude offset and scale-errors

Fig. 5 shows the photometric comparison between good-quality single–single matches within the common area for $B_{\rm MGC} - B_{\rm SCOS}$ (top), $B_{\rm MGC} - B_{\rm 2dF}$ (second from top), $B_{\rm MGC} - B_{\rm SDSS-DR1}$ (third from top) and $B_{\rm MGC} - B_{\rm SDSS-EDR}$ (bottom). Note that the 2dFGRS, SCOS, SDSS-EDR and SDSS-DR1 magnitudes were transformed according to the colour equations in Section 2.5 using the appropriate SDSS colour or SCOS colour for each individual galaxy. The photometric differences between the surveys are summarized in Table 2. The mean error in the photometry is ∼0.035 mag for the comparison of MGC to the other surveys, with less than 0.01 mag

Table 4. Summary of photometric differences as a function of surface brightness. This table lists the offset, average standard deviation per galaxy, the best linear fitting parameters a and b from equation (13) and the best quadratic fitting parameters α, β and γ from equation (14).

Data	Mean	σ	a	b	χ^2_ν	α	β	γ	χ^2_ν
MGC–2dF	0.035	0.142	0.053	0.096	35.1	0.073	0.081	−0.041	1.44
MGC–SCOS	0.032	0.108	0.040	0.026	37.5	0.057	0.012	−0.036	1.65
MGC–EDR	0.032	0.094	0.031	−0.016	22.5	0.039	−0.025	−0.015	1.29
MGC–DR1	0.039	0.086	0.039	−0.018	28.0	0.039	−0.026	−0.016	1.09
2dF–DR1	0.004	0.151	−0.018	−0.126	15.9	−0.031	−0.113	0.026	2.15
SCOS–DR1	0.005	0.103	−0.007	−0.056	17.0	−0.016	−0.043	0.022	2.22
DR1–EDR	−0.007	0.037	−0.008	0.0003	2.11	−0.008	0.002	0.001	1.06
SCOS–EDR	−0.002	0.107	−0.015	−0.057	17.3	−0.024	−0.043	0.022	3.94
2dF–EDR	−0.003	0.154	−0.024	−0.125	16.1	−0.037	−0.113	0.026	2.69
SCOS–2dF	0.001	0.086	0.012	0.070	8.10	0.015	0.068	−0.006	5.83

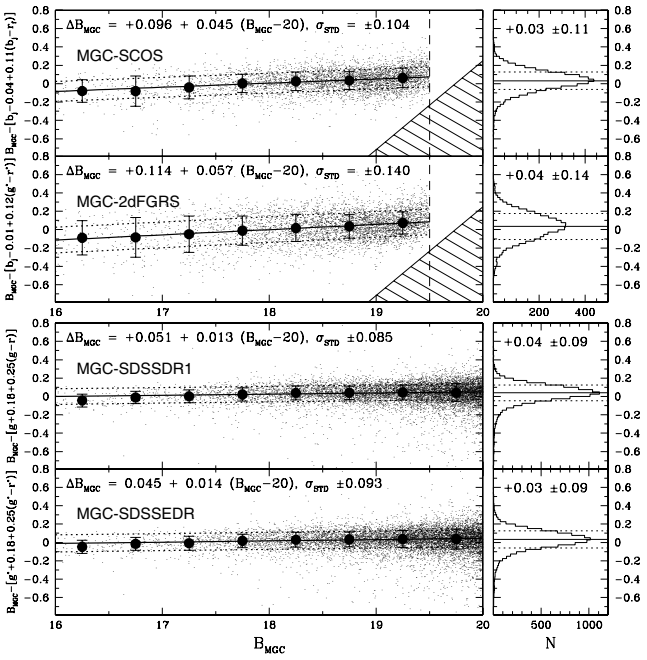

Figure 5. A comparison of photometry between MGC and SCOS (top panel), 2dFGRS (second panel), SDSS-DR1 (third panel) and SDSS-EDR (bottom panel). The left panels show the magnitude dependence along with the robust estimate of the best-fitting line via a chi-squared fit to the 3σ clipped standard deviation in each bin. The standard deviation quoted with the scale error is the standard deviation after subtracting this scale error. The right-hand panels show the histogram of the photometric differences with the 3σ clipped mean and standard deviations marked. See Table 2 for more details.

difference between these other surveys. Since 2dFGRS and SCOS have been calibrated to the SDSS-EDR, this latter result is not surprising. Thus[3] $B_{\rm MGC} - B_{\rm 2dF} = 0.035 \pm 0.005$ mag with a standard deviation per galaxy of 0.142 mag, $B_{\rm MGC} - B_{\rm SCOS} = 0.032 \pm 0.005$ mag with a standard deviation per galaxy of 0.108 mag, $B_{\rm MGC} - B_{\rm SDSS-\mathit{EDR}} = 0.032 \pm 0.005$ mag with a standard deviation per galaxy of 0.094 mag and $B_{\rm MGC} - B_{\rm SDSS-\mathit{DR1}} = 0.039 \pm 0.005$ mag with a standard deviation per galaxy of 0.086 mag.

[3] While the random errors between the MGC and 2dFGRS account for an error of 0.002 mag only, the colour equations in Fukugita et al. (1996), Smith et al. (2002) and Blair & Gilmore (1982) are only quoted to two decimal places, ±0.005 mag.

Since the 2dFGRS photometry and SCOS were taken from the same original UKST plates and the SDSS-DR1 is an update of the SDSS-EDR from the same CCDs, there are only three independent data sets. The best versions of these are the MGC, SCOS and SDSS-DR1. We will concentrate on the comparisons between these three, with brief asides on the 2dFGRS and SDSS-EDR, since there are many publications that use photometry from these data sets. From robust estimation via minimization of the mean deviations (including 3σ clipping) we determine the scale errors between the different data sets. We fit the following equation, and summarize the fits in Table 2:

$$\Delta m = a + b(B_{\rm MGC} - 20). \quad (12)$$

There is a 1.3 per cent scale error between the MGC and DR1 and a 4.5 per cent scale error between the MGC and SCOS. However, there is only a 2.1 per cent scale error between SCOS and DR1. The reason these do not add up is the non-linearity in the scale error between MGC and DR1, as can be seen from the large χ^2_ν value. If we select objects over the same magnitude range, $16 < B_{\rm MGC} < 19$, the three surveys become compatible, with the significant change coming from an increased scale error between MGC and DR1 (2.7 per cent). However, at the faint end, $19 < B_{\rm MGC} < 20$, the scale error is both small, 0.6 per cent, and linear. The SDSS-EDR has the same scale errors as the DR1, but is fainter by 0.007 mag and has a greater scatter ($\sqrt{\sigma({\rm EDR})^2 - \sigma({\rm DR1})^2} = 0.04$ mag). The 2dFGRS has a very large scale error compared to the MGC (almost *6* per cent), but is only 1.2 per cent different from SCOS, against which it was calibrated. The scale errors are larger, typically 2 ± 1 per cent at the bright end, $16 < B_{\rm MGC} < 19$, than the faint end, suggesting calibration problems associated with non-linearities, saturation or fewer standard stars. As we will show in Section 4.2, much of the variation is due to errors that are a function of surface brightness.

The 3σ clipped standard deviation (STD) of the overall magnitude variance appears as expected between the MGC and 2dFGRS data sets ($\sigma_{\rm STD} = \pm 0.14$ versus expected $\sigma_{\rm EXP} = \pm 0.15$) but worse than expected ($\sigma_{\rm STD} = \pm 0.09$ versus $\sigma_{\rm EXP} = \pm 0.04$) between the MGC and SDSS-DR1. SCOS has a smaller variance with respect to the MGC than 2dFGRS, while the SDSS-DR1 has a smaller variance than the SDSS-EDR, demonstrating the improved photometry in both catalogues.

To investigate whether this latter discrepancy may be due to systematic zero-point (ZP) offsets between the individual MGC fields, we show the equivalent trend for stars (Fig. 6, upper panels) and the ZP offset and standard deviation (Fig. 6, lower panels) per MGC field (using stars only). We then correct each individual magnitude

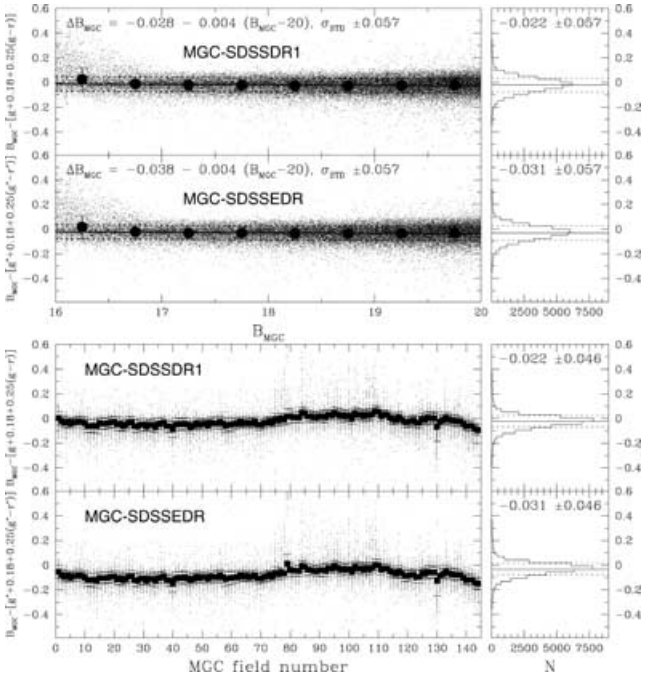

Figure 6. A comparison of the MGC and SDSS stellar photometry. The top panel shows the difference in photometry as a function of magnitude for the SDSS-DR1, where there is a 0.4 per cent scale error, show by the best-fitting lines and a standard deviation of 0.057 mag. The offset, −0.022 mag, appears different from the galaxy photometry, but when it is corrected for aperture differences it becomes (0.044 ± 0.005) mag, cf. (0.039 ± 0.005) mag. The similar plot for the SDSS-EDR is shown in the second from top plot. The only significant difference is in the offset, which is −0.031 mag. Table 3 summarizes the offsets and fits to the scale error. In the third and fourth panels we show the difference in photometry as a function of MGC field number, to determine the uncertainty due to zero-point errors across the MGC for the SDSS-DR1 and SDSS-EDR respectively. When we measure the mean standard deviation in each field we find that it is 0.046 mag, suggesting that the MGC field offsets may be responsible for some fraction (ΔZP ∼ ±0.035 mag) of the general photometric discrepancy. The histograms to the right of the third and fourth panels show the stellar population if the mean of each field is fixed to be the mean of the whole distribution.

by its respective field offset and rederive a ZP-corrected 3σ clipped mean for the full sample with a standard deviation ±0.046. This suggests that residual ZP offsets in the MGC *may* be at the level of up to ±0.035 mag, depending on variations across the SDSS, and therefore responsible for some fraction of this error. In Liske et al. 2003 we find a standard deviation of ±0.023 mag in the offsets between adjacent fields, with the most significant change occurring at field 74, as seen in Fig. 6. The scale error and variance error for stars are only improved marginally (<0.001 mag) between the SDSS-EDR and SDSS-DR1. The DR1 stellar magnitudes are 0.009 brighter than those in the EDR, compared to 0.007 mag brighter in the galaxy sample.

The larger variance for galaxies over stars suggests an additional 'galaxy measurement' error of ±0.06. This 'galaxy measurement' error consists in part of the increased signal-to-noise ratio per pixel since galaxies are more extended than stars and also the expected variations between Kron and Petrosian magnitudes, which are anywhere from +0.03 mag for an exponential profile to −0.12 mag for a de Vaucouleur's profile. It is difficult to calculate how large each component is, but it seems unlikely that the variations between Kron and Petrosian would count for less than ±0.03, since this is the smallest expected variation for a particular galaxy, and could easily account for ±0.04 or ±0.05. This implies that improved consistency in galaxy photometry must come from a unified approach to galaxy photometry.

The offset in the stellar magnitudes between the MGC and SDSS-DR1 is $B_{\rm MGC} - [g + 0.178 + 0.251(g - r)] = -0.022$ mag, which is significantly different from the offset in the galaxy magnitudes between the MGC and SDSS-DR1, $B_{\rm MGC} - [g + 0.178 + 0.251 (g - r)] = 0.039$ mag. The stars can be approximated by a Gaussian profile, and the expected offset between the Kron and Petrosian magnitudes for Gaussian profiles is $m_{\rm Kron} - m_{\rm Pet} = -0.066$ mag. Thus the relative stellar magnitudes should be corrected by 0.066 mag, giving a final value of $B_{\rm MGC} - [g + 0.178 + 0.251(g - r)] = (0.044 \pm 0.005)$ mag with an individual scatter of 0.046 mag for stars in the sample. The stellar and galaxy photometry agree to 0.005 mag.

For SCOS, 2dFGRS and SDSS comparisons we also find a variation in the variance as a function of magnitude, as indicated on Fig. 5 by the large solid data points (zero-point offset per 0.5 mag) and error bars (one 3σ-clipped standard deviation). It is worth noting that the 2dFGRS shows larger photometric variance at brighter magnitudes whereas the SDSS shows increasing variance at faint magnitudes as one would expect for decreasing signal-to-noise ratio data. SCOS shows both increasing variance at brighter and fainter magnitudes, with a minimum variance at $B_{\rm MGC} \sim 18.25$ mag.

4.2 Photometric variation with surface brightness

Fig. 7 shows the photometric variation as a function of effective surface brightness as defined in Section 2.1. We fit the magnitude errors with the following equations:

$$\Delta m = a + b(\mu_{\rm eff} - 23), \tag{13}$$

$$\Delta m = \alpha + \beta(\mu_{\rm eff} - 23) + \gamma(\mu_{\rm eff} - 23)^2. \tag{14}$$

None of the comparisons have good fits to equation (13), but almost all have good fits to equation (14), indicating substantial non-linearities with surface brightness. Since the MGC is deeper than SDSS, 2dFGRS and SCOS, it is expected that both β and γ will be small and negative, i.e. low surface brightness objects will be systematically fainter in the shallower surveys.

For the comparison between the MGC and the 2dFGRS, we see a large positive β, indicating a significant error in HSBGs with galaxies at the 10th percentile value of $\mu_{\rm eff}$ (21.5 mag arcsec^{-2}) offset from the mean by −0.18 mag, $B_{\rm MGC} - B_{\rm 2dFGRS}$. The LSBGs have magnitudes closer to the mean value, with the largest offset (+0.08 mag) at the 90th percentile value of $\mu_{\rm eff}$ (24.2 mag arcsec^{-2}). Since the HSBGs are the most affected, the error is probably caused by non-linearities in the plates that have not been completely corrected during the calibration process. Any studies that utilize the 2dFGRS photometry for structural analysis of the galaxy population (e.g. Cross et al. 2001) are thereby compromised. The SCOS data have a significant non-linearity too, $\gamma = -0.04$, but without the large linear error also evident in the 2dFGRS data. This results in an offset of ∼ −0.09 mag at 21.5 mag arcsec^{-2} and ∼ − 0.02 mag at 24.2 mag arcsec^{-2}.

In the MGC–SDSS comparison there is a small error at the low surface brightness end, $\mu_{\rm eff} > 24$ mag arcsec^{-2}. This error is ∼−0.06 mag difference from the EDR and ∼ − 0.07 mag difference in the DR1 at the 90th percentile value of $\mu_{\rm eff}$ (24.4 mag arcsec^{-2}).

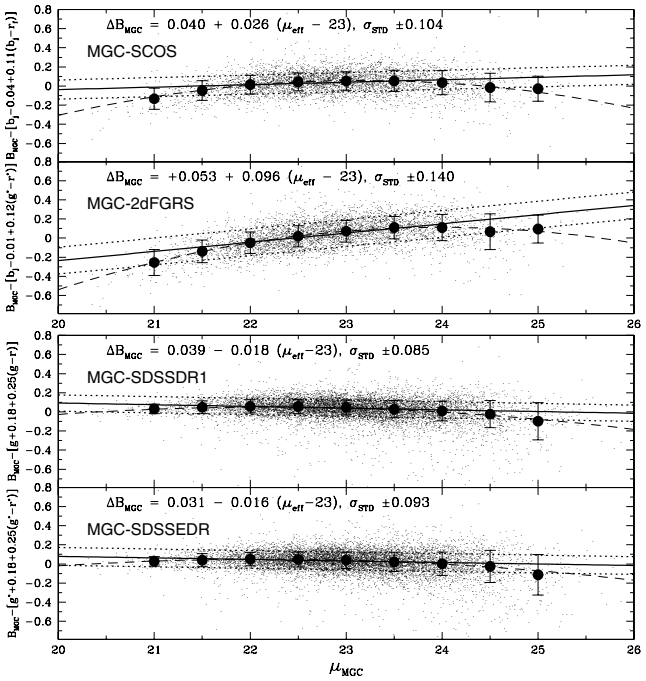

Figure 7. A comparison of the photometry between MGC and SCOS (top), MGC and 2dFGRS (second from top), MGC and SDSS-DR1 (third from top) and MGC and SDSS-EDR (bottom), as a function of effective surface brightness. The best linear fit, via (3σ) χ^2 minimization, is shown by the solid lines. However, in each case a quadratic fit, shown by the dashed line, gives a better fit. Table 4 gives the parameters for all the fits. Each panel gives the best linear fit and standard deviation after removing this fit.

The error is as one might expect when comparing a deeper data set with a shallower data set and suggests that some flux is missing in the outskirts of LSBGs in the SDSS-EDR data. While Kron and Petrosian magnitudes have little or no surface brightness dependence over a wide range of surface brightness, inevitably they will miss flux from galaxies close to the detection threshold since the profiles used to calculate the best aperture will be systematically miscalculated at very low signal-to-noise ratios.

Comparisons between the other surveys indicate similar results: the deeper survey finds more flux at the low surface brightness end, and there is a large ∼10 per cent error in the 2dFGRS with surface brightness and a smaller ∼4 per cent error in SCOS with surface brightness. From Figs 12 and 14 it is clear that bright galaxies are typically HSBGs. The large scale errors seen in the 2dFGRS and SCOS are due to these errors with surface brightness.

4.3 Photometric accuracy of known LSBGs

As a slight digression we briefly address the specific question of the photometric accuracy of LSBGs. Impey et al. (1996) published a catalogue of luminous low surface brightness objects from stacked APM scans in the equatorial region. From their full sample we note that 17 have positions inside the common MGC–2dFGRS–SDSS region. Of these we find matches for all 17 from within the MGC and the SDSS, and for 15 within the 2dFGRS. One of the missing 2dFGRS objects was listed in Impey et al. as fainter than the 2dFGRS magnitude limit, although both the MGC and SDSS magnitudes were above this limit. The other 2dFGRS failed match was close to a bright star and is most likely a misclassification or failed deblend.

The SDSS-EDR found multiple matches for seven of the objects. Table 5 shows the LSBG sample and the corresponding MGC matches for each survey, along with the best B_J magnitude for each of the data sets. Fig. 8 shows a montage of these 17 objects from the MGC data base. The magnitude zero-point offset and 3σ clipped standard deviations are: $B_{\rm LSBG} - B_{\rm MGC} = +0.22 \pm 0.32$, $B_{\rm LSBG} - B_{\rm SCOS} = +0.07 \pm 0.32$, $B_{\rm LSBG} - B_{\rm 2dF} = +0.21 \pm 0.31$, $B_{\rm LSBG} - B_{\rm SDSS-EDR} = -0.17 \pm 0.65$ and $B_{\rm LSBG} - B_{\rm SDSS-DR1} = -0.16 \pm 0.57$ respectively. The MGC and 2dFGRS recover similar results, SCOS has a similar scatter but is 0.2 mag fainter, and both the SDSS-EDR and SDSS-DR1 are 0.2 mag fainter than SCOS with greater scatter than the other three. We also note from Fig. 7 that the $\Delta(B_{\rm MGC} - B_{\rm SDSS})$ shows a larger dispersion than the $\Delta(B_{\rm MGC} - B_{\rm 2dF})$ in the faintest surface brightness bin. This suggests that SDSS-EDR

Table 5. A comparison of photometric matches between the three surveys and the 17 low surface brightness objects from (Impey et al. 1996, ISIB) within the common region. Objects marked with '*' have multiple components in the SDSS. Each magnitude is the combination of all the components. All the photometry is in $B_{\rm Johnson}$.

ISIB ID	RA (deg)	Dec. (deg)	B	$\mu_{\rm o}$	$\mu_{\rm eff}$	MGC ID	$B_{\rm MGC}$	$B_{\rm SCOS}$	$B_{\rm 2dF}$	$B_{\rm EDR}$	$B_{\rm DR1}$
1035+0014	159.606	−0.0183	16.60	22.40	24.60	MGC90026	16.44	16.78	16.49	17.06*	16.74*
1042+0020	161.287	0.0753	16.20	21.40	23.40	MGC11548	16.43	16.41	16.48	16.67*	16.69*
1043+0018	161.561	0.0500	16.20	21.40	22.20	MGC11695	15.79	15.80	15.85	15.88	15.93
1045+0014	162.082	−0.0225	16.20	21.80	22.70	MGC11884	16.27	16.02	15.95	16.39	16.21
1102+0019	166.166	0.0572	17.30	24.10	25.50	MGC16030	17.00	17.51	17.47	17.83*	17.39*
1125+0025	172.123	0.1436	17.60	23.00	23.80	MGC20736	17.39	17.43	17.11	17.54	17.52
1129+0013	172.994	−0.0508	16.30	22.30	23.50	MGC21656	15.92	16.31	15.85	16.15	16.20
1216+0029	184.858	0.2150	17.00	22.90	25.20	MGC31502	16.82	16.69	16.63	17.73*	17.82*
1221+0001	185.926	−0.2575	18.40	23.90	25.80	MGC32646	18.01	18.20	18.20	18.47*	18.63*
1221+0020	186.127	0.0708	17.60	23.70	25.40	MGC32544	17.01	17.41	17.22	17.34	17.45
1247+0002	192.519	−0.2339	19.60	26.40	27.30	MGC38179	17.74	–	–	18.16*	19.17*
1310+0013	198.187	−0.0406	16.60	22.30	23.90	MGC43127	17.03	17.16	16.86	18.36	18.34
1405+0006	212.132	−0.1272	15.20	20.60	21.80	MGC56580	15.42	15.55	15.44	15.59*	15.68*
1434+0020	219.160	0.1164	17.50	22.90	24.50	MGC64880	17.21	17.22	16.92	17.28	18.32
1437+0001	219.998	−0.1869	18.50	24.20	25.40	MGC66574	18.02	18.36	18.26	19.14	18.13
1442+0026	221.355	0.2339	16.70	24.10	24.30	MGC90173	16.44	–	–	16.51	16.53
1158+0023	180.159	0.1106	19.00	24.40	25.00	MGC27147	18.25	18.29	18.31	19.30	18.54

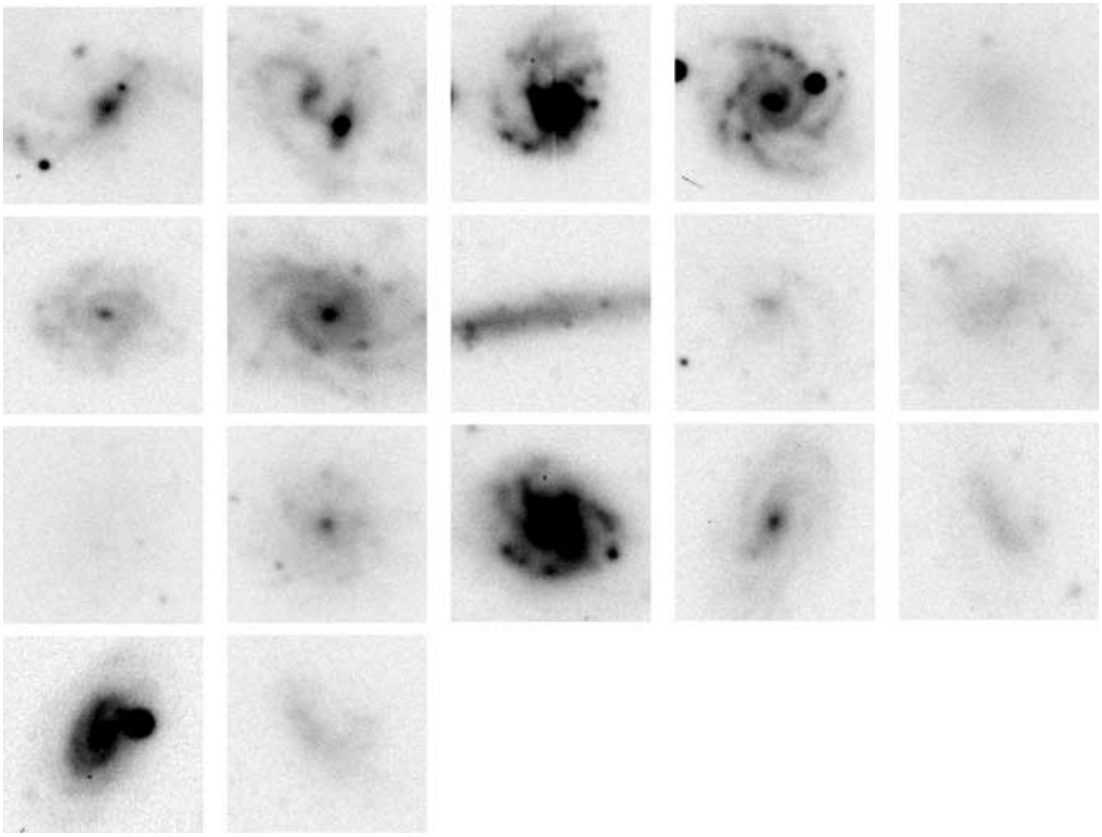

Figure 8. The Impey et al. (1996) LSBGs in the MGC region. Each image is 33 × 33 arcsec^2. The grey-scale varies from 21 mag arcsec^{-2} (black) to the 3σ variation in noise above the sky background (white).

photometry should be considered questionable for objects with $\mu_{\rm eff} > 24.5$ mag arcsec^{-2}. Fig. 9 shows the Δm versus $\mu_{\rm eff}$ derived from Table 5, which clearly shows the degradation of photometric accuracy in the SDSS data as a function of effective surface brightness (filled and open circles representing SDSS-EDR and SDSS-DR1 data respectively). We also note the slightly upward trend in $\Delta(B_{\rm LSBG} - B_{\rm MGC})$ with increasing effective surface brightness, suggesting that the Impey et al. (1996) magnitudes themselves may be underestimating flux at the very low surface brightness end. In particular, the lowest LSBG (1247+0002), identified in both the MGC and SDSS-EDR, but not in the 2dFGRS, is considerably brighter in MGC-BRIGHT and the SDSS-EDR than listed in Impey et al.

5 CLASSIFICATION RELIABILITY

All galaxies in MGC-BRIGHT have been visually inspected and artefacts reclassified, merged objects deblended, and over-deblends reformed. The MGC should therefore be considered robust. The 2dFGRS and SDSS-EDR data sets use automated detection and classification algorithms over this magnitude range. It is therefore important to ascertain some independent measure of the reliability of these large-scale surveys. Here we consider the accuracy of the automated classifiers in terms of star–galaxy separation, and contamination of the galaxy catalogues by stars or artefacts and galaxy incompleteness.

5.1 Star–galaxy classification accuracy

Although the 2dFGRS data base is supposed to include only objects classified as galaxies, it is known to be contaminated by stars at the 5.4 per cent level (cf. Norberg et al. 2001).

We calculated the stellar contamination using the 2dFGRS–MGC catalogue. There are 5241 good 2dFGRS objects matched to MGC objects.[4] Of these, 368 are multiple matches, (7.0 ± 0.4) per cent, 178 are single stars and 4695 are single galaxies. The fraction of 2dFGRS mismatches is not correlated with magnitude, as also noted in Norberg et al. (2002b). The fraction of single systems that are stars is (3.7 ± 0.3) per cent. The total fraction of 2dFGRS objects containing stars is (6.8 ± 0.3) per cent and the fraction in which the main component is a star is (5.2 ± 0.3) per cent. This agrees with the measurement of stellar contamination determined in earlier papers and by the spectroscopic data (Colless et al. 2001). This indicates that while the star–galaxy separation algorithm does very well on individual stars and galaxies, it breaks down on close pairs.

The SDSS-EDR data base includes stars and galaxies classified according to the criterion described in Stoughton et al. (2002). For our sample of 9795 MGC galaxies ($16 < B_{\rm MGC} < 20$ mag), we find the following matches from the SDSS-EDR data base: 9656 galaxies, 20 stars and 119 non-detections. For our sample of 36 260 MGC stars we find, in the SDSS-EDR data base: 305 galaxies and 35 726 stars, leaving 229 non-detections. Since we have spectra from various sources, it is possible to test the reliability of each classification.

We can find the stellar contamination by dividing the number of objects classified as galaxies with $z < 0.002$ by the total number

[4] In a previous section we stated that there were 5285 2dFGRS objects matched to MGC objects. In that section we gave the number of objects for $[b_{\rm 2dF} - 0.012 + 0.121(g^* - r^*)] > 16$ mag, so that the number of non-matches could be calculated. Here we give the number of objects for $B_{\rm MGC} > 16$ mag, since the MGC is our yardstick.

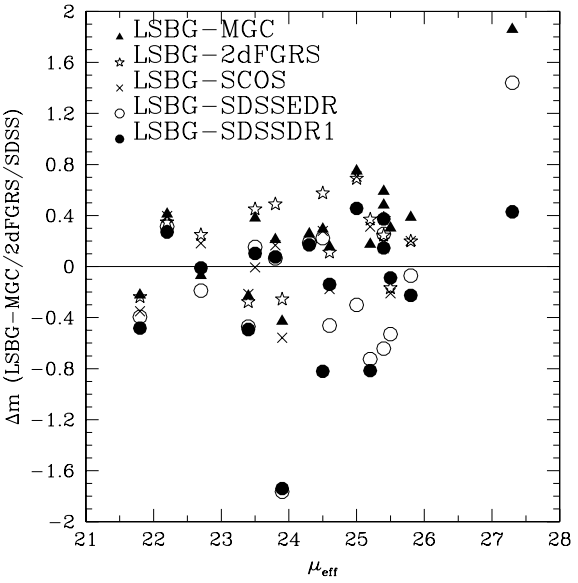

Figure 9. The photometric error between the surveys and the Impey et al. (1996) LSBGs in the common region as a function of effective surface brightness.

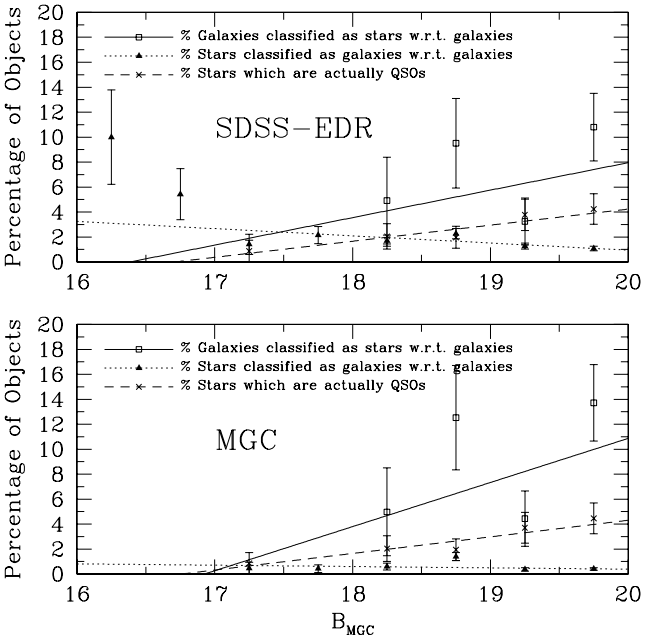

Figure 10. This plot shows misclassifications of stars and galaxies in the MGC and SDSS-EDR as a function of magnitude. The filled triangles show the percentage of stars contaminating the galaxy catalogue, as a function of magnitude. The dotted lines show the best linear fit to these data. The open squares show the number of misclassified galaxies as a percentage of the galaxy catalogue, as a function of magnitude. The solid lines show the best linear fit to these data. The crosses show the fraction of 'stars' that are in fact QSOs as a function of magnitude. The dashed lines show the best linear fit to these data.

of objects classified as galaxies. This measurement may be biased since the spectroscopic completeness varies with magnitude (see Section 6). We remove this bias by calculating this fraction as a function of magnitude ($f_{\rm stcon}(B_{\rm MGC})$) and then multiplying by the total number of galaxies, to give the expected number of stellar contaminants at that magnitude. Furthermore, we only use redshift data from the 2dFGRS and our own redshift survey as these are only selected by magnitude and not colour.

The fraction of stellar contamination at each magnitude is plotted as the triangles in Fig. 10. The best linear fit to the data is shown as the dotted line. The total stellar contamination is equal to the integral of this function over the range $16 < B_{\rm MGC} < 20$ mag:

$$N_{\rm stcon} = \int_{16}^{20} \frac{N_{{\rm g},z<0.002}(m)}{N_{{\rm g,all}z}(m)} N_{\rm g}(m)\,{\rm d}m, \tag{15}$$

where $N_{{\rm g},z<0.002}(m)$ is the number of objects classified as galaxies with $z < 0.002$, $N_{{\rm g,all}z}(m)$ is the number of objects classified as galaxies with a measured redshift, and $N_{\rm g}(m)$ is the total number of objects classified as galaxies, all as a function of magnitude. $N_{\rm stcon}$ is the total stellar contamination. In the MGC the stellar contamination is (0.47 ± 0.07) per cent and it is (1.33 ± 0.11) per cent in the SDSS-EDR.

We perform similar calculations to find the number of galaxies misclassified as stars with respect to galaxies,

$$N_{\rm misclgal} = \int_{16}^{20} \frac{N_{{\rm s},0.002<z<0.4}(m)}{N_{{\rm s,all}z}(m)} \frac{N_{\rm s}(m)}{N_{\rm g}(m)} N_{\rm g}(m)\,{\rm d}m, \tag{16}$$

and the number of stellar objects that are quasars (QSOs),

$$N_{\rm frqso} = \int_{16}^{20} \frac{N_{{\rm s},z>0.4}(m)}{N_{{\rm s,all}z}(m)} N_{\rm s}(m)\,{\rm d}m. \tag{17}$$

In equations (16) and (17), $N_{\rm misclgal}$ is the total number of misclassified galaxies, $N_{\rm frqso}$ is the total number of QSOs, $N_{{\rm s},0.002<z<0.4}(m)$ is the number of objects classified as stars with $0.002 < z < 0.4$, $N_{{\rm s},z>0.4}(m)$ is the number of objects classified as stars with $z > 0.4$, $N_{{\rm s,all}z}(m)$ is the number of objects classified as stars with a measured redshift, $N_{\rm s}(m)$ is the total number of objects classified as stars, $N_{\rm g}(m)$ is the total number of objects classified as galaxies, all as a function of magnitude.

However, since the QSO spectroscopic surveys targeting the stellar populations are mainly colour-selected, the objects from these surveys are not representative of the full stellar population. In our own redshift survey (MGCZ), we targeted the whole population of stars and galaxies with $B_{\rm MGC} < 20$ mag in some MGC spectroscopic tiles. We use data from two such tiles (each tile is a separate pointing of the 2dF instrument, and has a diameter of 1.95 deg). The MGCZ targets the remaining stellar targets once the data from other spectroscopic surveys has been tallied, so it is important to use all the spectroscopic data available in these fields, not just MGCZ. This introduces some bias from the colour-selected surveys if the sample is not complete. These tiles contain 1887 stars, of which there are 1403 spectra from MGCZ and 53 spectra from other surveys. We find that ∼2 per cent of these stars have redshifts of galaxies, leading to a galaxy misclassification rate of (6.6 ± 1.3) per cent in the MGC and (5.3 ± 1.0) per cent in the SDSS-EDR. We estimate that (5.6 ± 1.3) per cent of galaxies in the 2dFGRS (galaxies in the MGC with $B_{\rm MGC} < 19.0$) are misclassified as stars. The fraction of QSOs in the MGC stellar catalogue is (2.1 ± 0.4) per cent and the fraction in the SDSS stellar catalogue is (2.2 ± 0.4) per cent. The effects of the bias from colour-selected surveys on the sample add an error of ∼0.1 per cent.

In each case the number of contaminants increases with magnitude. However, the fraction of stellar contamination of the galaxy catalogue does not vary significantly with magnitude. The fraction of misclassified galaxies and the fraction of QSOs amongst the stars rise more steeply.

Table 6. A summary of objects in the SDSS-EDR with no counterpart in the MGC.

Reason	No. of stars	No. of galaxies	Percentage of stars	Percentage of galaxies
Failed match	101	191	0.29	1.90
Badly blended	79	20	0.23	0.20
Smudges near bright objects	0	6	0.00	0.06
Detected but not catalogued	119	66	0.34	0.65
Artefacts	36	46	0.10	0.45
Total	335	329	0.96	3.20

One caveat to the method above is the cut-off redshift for stars and galaxies, $z = 0.002$. This was chosen based on the distribution of low-redshift objects in the 2dFGRS and assumes a Gaussian distribution of velocities for stars in the Milky Way. Since the Milky Way is a multicomponent system, this limit may miss some of the halo stars. While there are a few objects just above the limit, which may turn out to be stars, this only reduces the numbers of misclassified galaxies by 22 per cent, from (6.6 ± 1.3) per cent to (5.1 ± 1.3) per cent in the MGC. It still leaves a significant fraction of misclassified galaxies. The misclassified galaxies will be discussed in more detail in a future paper (Liske et al., in preparation).

5.2 Artefacts

Of the 49 2dFGRS objects that were not matched to MGC objects, 34 were 2dFGRS eyeball rejects, i.e. inspections of the plates had already revealed them to be artefacts, eight were not visible in Digital Sky Survey images (from the same Schmidt plates) and seven looked like asteroids or satellite trails in the DSS images. None of these objects appeared in the SDSS. Thus all the extra 2dFGRS objects are accounted for and any objects missing from the MGC are also missing in the 2dFGRS.

The SDSS-EDR contains 10 213 galaxies and 34 779 stars in the range ($16 < B_{\rm MGC} < 20$ mag), of which 329 galaxies and 335 stars had no apparent counterparts in the MGC. These were checked by eye. They were missed for various reasons (see Table 6). In some cases (292) the matching algorithm failed, and in another 99 cases the object was badly blended with a star, leading to a disagreement in the deblending. There were another six faint smudges, near bright objects. There were 119 'stars' and 66 galaxies seen in MGC images that do not appear in the MGC catalogues. This represents 0.35 per cent of the stars and 0.67 per cent of the galaxies. These missing objects are close to bright stars and suggest that the exclusion regions are too conservative.

Finally, 46 galaxies and 36 stars had no counterparts in MGC-BRIGHT or MGC-FAINT ($B_{\rm MGC} < 24$ mag) or flux in the images and are therefore artefacts. The proportion of artefacts appears to be (0.45 ± 0.07) per cent for galaxies and (0.10 ± 0.02) per cent stars. Table 7 summarizes the proportions of stellar contamination, misclassified galaxies and artefacts in each survey.

6 INCOMPLETENESS

The magnitude limit of the 2dFGRS catalogue is nominally $b_{\rm 2dF,old,lim} = 19.45$ mag. However, the photometry of objects in the 2dFGRS has been revised since the target catalogues were produced, so there is not a single magnitude limit. Two of the plates (UKST 853 and 866) have particularly bright limiting magnitudes, $b_{\rm 2dF,lim} < 19.18$ mag, so we have removed these plates when testing the completeness. The plates are removed by selecting MGC galaxies in the range $153^\circ.145 < {\rm RA} < 213^\circ.145$ and ${\rm RA} > 218^\circ.145$. Galaxies in this part of the 2dFGRS have $b_{\rm 2dF,lim} \geqslant 19.23$ mag. This corresponds to $B_{\rm MGC} = 19.365$ mag. If we test the completeness at $B_{\rm MGC} = 19.0$ mag, 2.56 standard deviations brighter than this limit, only 0.5 per cent of the 2dFGRS data at this magnitude (i.e. <5 objects) will be missing due to random errors.

Table 7. A summary of the classification reliability of the 2dFGRS and SDSS-EDR galaxy catalogues from comparison with the MGC. Each number gives the fractions as a percentage with respect to the galaxy population.

Catalogue	Stars classified as galaxies	Gals classified as stars	Artefacts
2dFGRS	5.2 ± 0.3	5.6 ± 1.3	0.9 ± 0.1
SDSS-EDR	1.3 ± 0.1	5.3 ± 1.0	0.45 ± 0.07
MGC	0.47 ± 0.07	6.6 ± 1.3	–

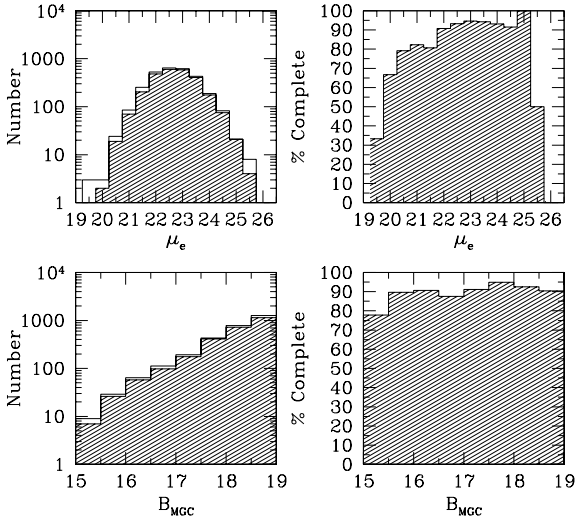

Figure 11. The variation of the incompleteness of the 2dFGRS with $B_{\rm MGC}$ (lower) and $\mu_{\rm eff}$ (upper). The left-hand plots show the histogram of the total number of galaxies in each bin (solid line), and the histogram of the number with redshifts (filled). The right-hand histogram shows the completeness percentage in each bin.

There are 2891 MGC galaxies in the correct RA range with $B_{\rm MGC} < 19.0$ mag. This catalogue was separated into objects with a 2dFGRS match and objects without. MGC objects that are a member of a multiple system of two or more MGC objects matched to a single 2dFGRS object were placed into the matched bin if they were the principal component and into the non-matched bin if they were a secondary component. There were 2646 matches, giving a completeness rate of (91.3 ± 1.8) per cent. The variation of incompleteness with magnitude is shown in Fig. 11. The variation is consistent with a constant incompleteness, so the incompleteness at $b_{\rm 2dF} = 19.45$ mag is ${\rm IC}_{b_{\rm j}19.45} = (8.7 \pm 0.6)$ per cent. This result matches the result from Norberg et al. (2002b), which gives a value ${\rm IC}_{b_{\rm j}19.0} = (9 \pm 2)$ per cent. It is marginally greater than the original APM expectation of 3–7 per cent incompleteness.

The variation with effective surface brightness is also shown in Fig. 11. For $22.5 < \mu_{\rm eff} < 24.5$ mag arcsec^{-2}, the completeness is fairly constant IC $\sim$ 5 per cent. The incompleteness of LSBGs

increases rapidly beyond $\mu_{\rm eff} = 25.0$ mag arcsec^{-2} and no 2dFGRS galaxies are seen with $\mu_{\rm eff} > 25.75$ mag arcsec^{-2}, as expected with an isophotal limit $\mu_{b_{\rm j,lim}} = 24.67$ mag arcsec^{-2} (see Cross et al. 2001) and an exponential profile ($\mu_{\rm eff} = \mu_0 + 1.124$ mag arcsec^{-2}). At the bright end, the incompleteness rises steadily. Since the incompleteness rises steadily for faint objects and also for high surface brightness objects, it would make sense if a significant proportion of the missing objects are both faint and high surface brightness, i.e. compact galaxies that looked like stars on the Schmidt plates.

The variation with surface brightness is consistent with the Norberg et al. (2002b) comparison between the 2dFGRS and SDSS-EDR, given that the peak in the surface brightness distribution of his sample is $\mu_{b_{\rm j}} = 22.2$ mag arcsec^{-2} and the peak in the surface brightness distribution of our sample is $\mu_{\rm e}$,$B_{\rm MGC} = 22.9$ mag arcsec^{-2}. At the high surface brightness end, we both measure a decrease in completeness at $\mu_{\rm e}B_{\rm MGC} \sim 21.7$ mag arcsec^{-2} ($\mu_{b_{\rm j}} \sim 21.0$ mag arcsec^{-2}). At the low surface brightness end, the decline in completeness appears to occur at a slightly different point, but is consistent with the errors and the incompleteness of the SDSS (see Section 6.2).

6.1 Types of galaxy missing from 2dFGRS

Fig. 12 shows all the galaxies $B_{\rm MGC} \leqslant 19.0$ mag plotted in the $B_{\rm MGC}$ versus $\mu_{\rm eff}$ plane. The lower horizontal line represents the limit at which LSBGs would be expected to be missed from the 2dFGRS.

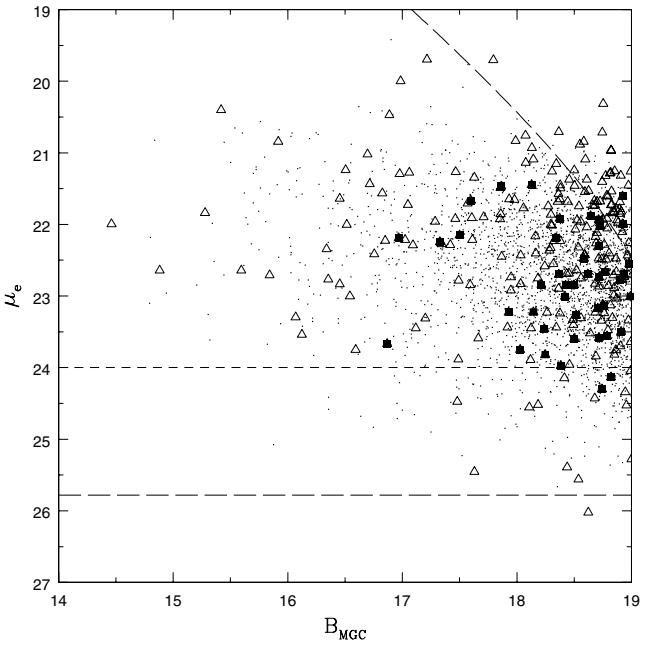

Figure 12. Plot of all galaxies $B_{\rm MGC} \leqslant 19.0$ in the $B_{\rm MGC}$ versus $\mu_{\rm eff}$ plane. The dots represent galaxies with 2dFGRS matches, the open triangles represent those without matches and the filled squares represent those without matches which are the secondary components of 2dFGRS matches. The lower horizontal line represents the theoretical limit at which 2dFGRS galaxies can be seen. The upper horizontal line represents the limit at which a significant fraction of 2dFGRS galaxies are being missed. Objects below this line are probably missed because of their low surface brightness. The curved line (top right) represents an exponential galaxy with a radius of 3.6 arcsec. More compact objects were excluded because they were classified as stars – see Cross et al. (2001).

The upper horizontal line represents the limit at which a galaxy is classified as an LSBG ($\mu_{\rm eff} > 24.0$ mag arcsec^{-2}). These galaxies make up 6.1 per cent of the population of missing galaxies. The curved line (top right) represents the rough star–galaxy separation line. This curve is the locus of disc galaxies with $r_{\rm iso} = 3.6$ arcsec when $\mu_{b_{\rm j,lim}} = 24.67$ mag arcsec^{-2}. While the APM detects objects with a minimum of 16 pixels, corresponding to 4 arcsec^2, the histogram of objects in the 2dFGRS has a minimum radius of $\sim$3.6 arcsec. The 17.8 per cent of objects faintwards of this line are more compact than this and are likely to be unresolved. The filled squares represent objects that are secondary components of 2dFGRS galaxies, missed because of poor deblending. These make up 17.4 per cent of missing galaxies, although two galaxies are missed because they are thought to be stars with poor deblending. These objects account for 39.7 per cent of missing objects.

We looked for the other 60 per cent of missing 2dFGRS objects in the full APM catalogue. The APM catalogue contains many objects that did not make the final 2dFGRS selection catalogue as a result of difficulties getting spectra: e.g. other nearby galaxies or stars. The rest of the missing 2dFGRS objects were compared to these objects. The excluded objects included blended objects, unresolved objects and some normal galaxies. After looking at these objects, it was discovered that (53 ± 5) per cent of all missing 2dFGRS objects were classed as blended, or were secondary objects matched to a 2dFGRS object, (18 ± 3) per cent were unresolved, (19 ± 3) per cent were normal galaxies and (6 ± 2) per cent were LSBGs.

Blended objects are those resolved by the APM which were still too close together for the 2dF spectrograph to be able to handle adequately. Secondary objects were those too close to another object to be resolved by the APM.

Pimbblet et al. (2001) have also looked at the completeness of the APM by matching it to Las Campanas/AAT Rich Cluster Survey (LARCS) data for four Abell clusters. They find a higher overall incompleteness rate, with 10–20 per cent of galaxies missing at all magnitudes, $b_{\rm 2dF} \leqslant 18.85$ mag, and $\sim$20 per cent missing for $b_{\rm 2dF} < 17.0$ mag. The denser environment of clusters might explain why a larger fraction of objects are missing in the LARCS data since one would expect more blends. However, Pimbblet et al. (2001) show that there is no increase in total fraction or blended fraction close to the cluster centres. They find that 60 per cent of missing objects are blends, 15 per cent were unresolved galaxies, 20 per cent are normal galaxies and 5 per cent are LSBGS. Pimbblet et al. also find the median merger distance for blends, which varies from (5.3 ± 0.9) arcsec in Abell 1084 to (8.6 ± 0.9) arcsec in Abell 22.

The LARCS group also determined why galaxies have been missed in the 2dFGRS. Missing blended, unresolved objects and LSBGs are easily understood, but it is difficult to comprehend why those galaxies classified as normal are missing. Pimbblet et al. (2001) found that these objects had been classified as 'stellar', 'blended' or 'noise' on APM R-band plates, which were used jointly with the $b_{\rm j}$ plates to classify objects. The original APM catalogues are complete for all galaxies apart from some LSBGs, secondary galaxies and poorly resolved galaxies (about 3.7 per cent of all galaxies, $B_{\rm MGC} < 19.0$ mag), but the 2dFGRS target catalogue is less complete, missing (8.7 ± 0.6) per cent of $B_{\rm MGC} < 19.0$ mag galaxies.

Finally Pimbblet et al. (2001) showed that the proportion of blends and unresolved galaxies missing in the 2dFGRS is constant with magnitude, whereas normal and LSBGs are missed predominantly at $b_{\rm 2dF} > 18.0$ mag. A modest increase in incompleteness is seen for fainter galaxies, but the uncertainties are such that the results are consistent with constant incompleteness.

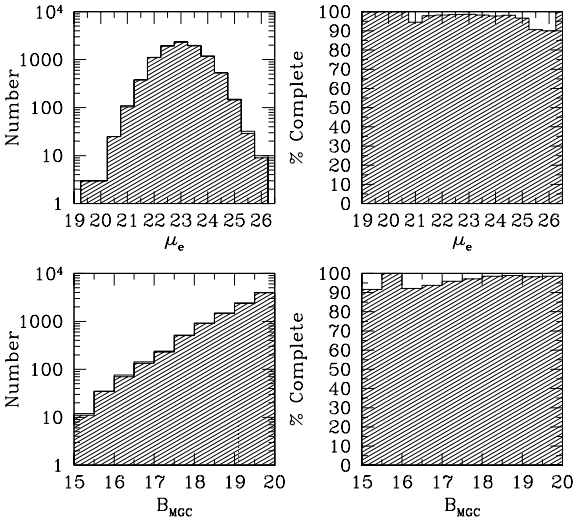

Figure 13. The variation of the incompleteness of the SDSS-EDR with $B_{\rm MGC}$ (lower) and $\mu_{\rm eff}$ (upper). The left-hand plots show the histogram of the total number of galaxies in each bin (solid line), and the histogram of the number with redshifts (filled). The right-hand histogram shows the completeness fraction in each bin.

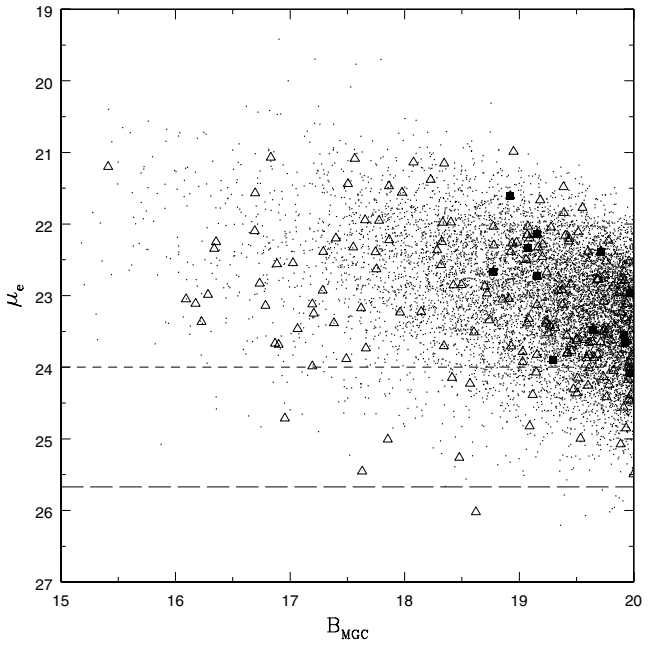

Figure 14. Plot of all galaxies $B_{\rm MGC} \leqslant 20.0$ in the $B_{\rm MGC}$ versus $\mu_{\rm eff}$ plane. The dots represent galaxies with SDSS-EDR matches, the open triangles represent those without matches and the filled squares represent those without matches which are the secondary components of SDSS-EDR matches. The lower horizontal line represents the theoretical limit at which SDSS-EDR galaxies can be seen.

6.2 Incompleteness of the SDSS-EDR

We have also checked the incompleteness of the SDSS-EDR. Out of 9795 MGC galaxies ($B_{\rm MGC} < 20$ mag), the overall incompleteness is (1.8 ± 0.1) per cent. Fig. 13 shows the photometric incompleteness of the SDSS-EDR as a function of $B_{\rm MGC}$. The incompleteness is never greater than *3* per cent at any magnitude. Fig. 13 also shows the photometric incompleteness of the SDSS-EDR as a function of $\mu_{\rm eff}$. The incompleteness is $\leqslant$5 per cent for $21.5 < \mu_{\rm eff} < 25.0$ mag arcsec^{-2}. It rises when $\mu_{\rm eff} > 25.0$ mag arcsec^{-2} due to the low signal-to-noise ratio of these galaxies in the SDSS. While only (2.0 ± 0.4) per cent of LSBGs with $\mu_{\rm eff} > 24.0$ mag arcsec^{-2} are actually missing, this represents (13.5 ± 2.8) per cent of all missing SDSS galaxies.

Fig. 14 shows the distribution of missing galaxies (open triangles) as a function of $B_{\rm MGC}$ and $\mu_{\rm eff}$. The filled squares show missing galaxies, where the MGC galaxy is the secondary component of an SDSS galaxy $(32.8 \pm 4.3$ per cent of cases).

6.3 Magnitude and surface brightness biases in incompleteness

It is important to select a region of parameter space with high completeness when measuring the space density. If a region has high photometric incompleteness, then many objects have been missed from the input catalogues, e.g. compact objects that are thought to be stars, LSBGs. We have no information about these objects and can only speculate on their importance to the overall luminosity and mass density. In regions where the photometric incompleteness is high, then the redshift incompleteness will also be high, but there can be additional regions where the photometric incompleteness is low, but the redshift incompleteness is high. This may be for a variety of reasons: low signal-to-noise ratio in the spectrograph, or objects that are only found in clusters may be missed preferentially because of the minimum separation of fibres.

Thus the calculation of the space density will only be robust in regions where both the photometric and the redshift completeness are high. In regions where the redshift completeness is low, the question is this: Have the missing objects got the same redshift distribution as those objects with redshifts? This may be a plausible assumption, but objects with spectral lines close to sky lines may be missed preferentially, or objects with weak emission or absorption may be missed in preference to those objects with strong lines. If the photometric incompleteness is high, not only do we have these problems, but we also have to wonder if there is redshift or other bias in the missing objects. As shown in Section 6.1, there are many blended objects and compact objects missing from the 2dFGRS. These may be preferentially missed from cluster environments where a lot of galaxies have a similar redshift. Thus the redshift distribution seen in that region of parameter space may be less clustered than the true redshift distribution.

Fig. 15 shows the photometric completeness of the combined 2dFGRS data set as a function of both magnitude and surface brightness. Fig. 16 shows the equivalent plot for the SDSS-EDR. In the case of the 2dFGRS, the completeness is very low (<40 per cent) for $B_{\rm MGC} > 19.5$ and also very low for faint HSBGs, which may be confused with stars. The SDSS-EDR on the other hand has very high completeness (>90 per cent) in virtually every bin.

Fig. 17 shows the redshift completeness of the 2dFGRS. Fig. 18 shows the redshift completeness of the SDSS-EDR. For the 2dFGRS the original spectroscopic magnitude limit was $b_{\rm 2dF} = 19.45$ mag, but this has now become a variable with plate number and dust correction. The analysis above showed that the limit for high completeness is $B_{\rm MGC} \sim 19.0$ mag. For the SDSS-EDR, the spectroscopic limit is $r^* = 17.7$ mag for most galaxies. The filter conversion equation is $B = g^* + 0.251(g^* - r^*) + 0.178$, which converts to $B_{\rm MGC} = r^* + 1.251(g^* - r^*) + 0.178$. Using a typical $(g^* - r^*) = 0.6$, $B_{\rm MGC,lim} = 18.7$ mag for the SDSS-EDR. However, the completeness may drop before this limit or after this limit because of the variation in colours of galaxies in the sample. It is apparent that the

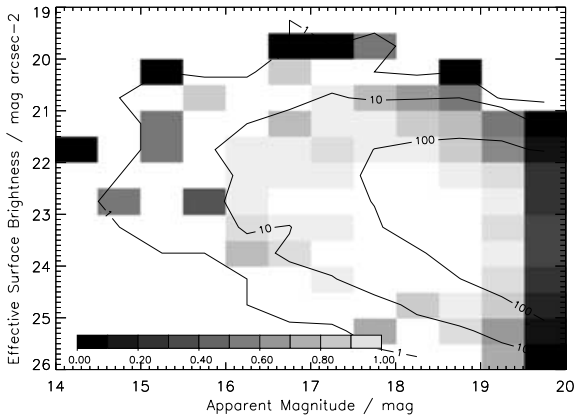

Figure 15. The photometric completeness of the 2dFGRS imaging catalogue as a function of $B_{\rm MGC}$ and $\mu_{\rm eff}$. The grey-scale represents the completeness fraction of galaxies. The contours represent the total number of MGC galaxies in each bin. Outside of the $N_{\rm tot} = 1$ line there are no data.

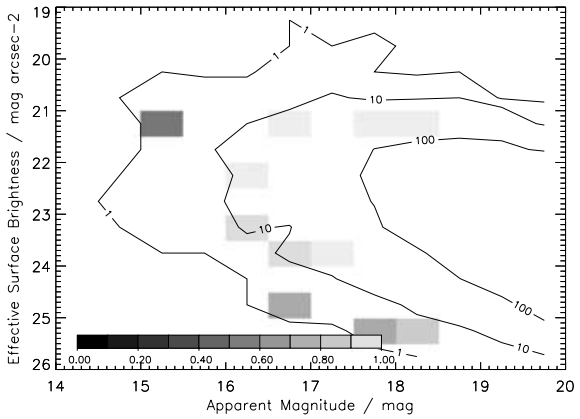

Figure 16. The photometric completeness of the SDSS-EDR imaging catalogue as a function of $B_{\rm MGC}$ and $\mu_{\rm eff}$. The grey-scale represents the completeness fraction of galaxies. The contours represent the total number of MGC galaxies in each bin. Outside of the $N_{\rm tot} = 1$ line there are no data.

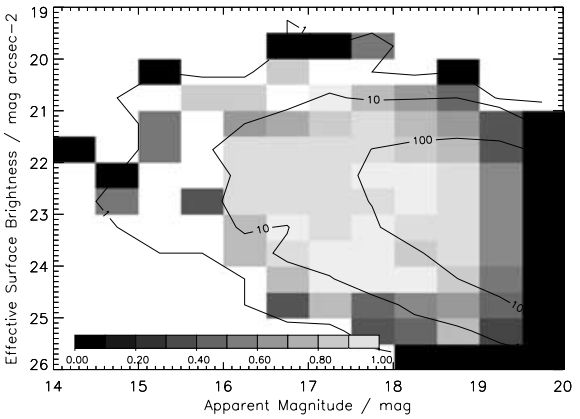

Figure 17. The redshift completeness of the 2dFGRS imaging catalogue as a function of $B_{\rm MGC}$ and $\mu_{\rm eff}$. The grey-scale represents the completeness fraction of galaxies. The contours represent the total number of MGC galaxies in each bin. Outside of the $N_{\rm tot} = 1$ line there are no data.

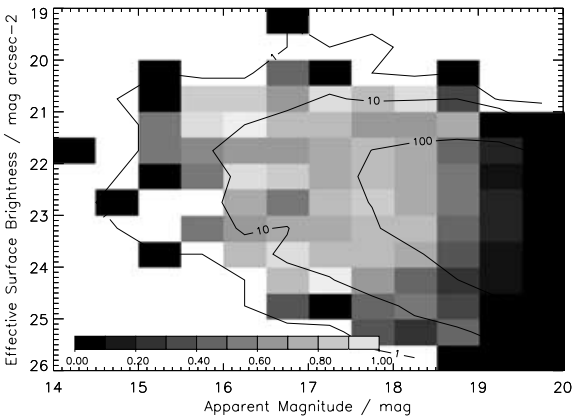

Figure 18. The redshift completeness of the SDSS-EDR imaging catalogue as a function of $B_{\rm MGC}$ and $\mu_{\rm eff}$. The grey-scale represents the completeness fraction of galaxies. The contours represent the total number of MGC galaxies in each bin. Outside of the $N_{\rm tot} = 1$ line there are no data.

redshift completeness of the SDSS-EDR falls off ∼0.5 mag brighter than the 2dFGRS. The 2dFGRS is more complete than the SDSS-EDR because it has been finished, whereas there are some small gaps in the SDSS-EDR spectroscopic release. In the MGC these gaps occur at 152.7 < RA < 153.4, 153.9 < RA < 155.5, 168.5 < RA < 170.5 and 203.0 < RA < 204.8. The spectroscopic sample of the SDSS-EDR was selected in the r^* filter, so bluer galaxies will have a brighter $B_{\rm MGC,lim}$ and redder galaxies will have a fainter $B_{\rm MGC,lim}$. It is not the overall redshift completeness that concerns us, but rather how the completeness varies with magnitude and surface brightness.

There is a reduced level of redshift completeness in both surveys for galaxies with $\mu_{\rm eff} > 24.5$ mag arcsec^{-2}, whereas the photometric completeness dropped most significantly for objects with $\mu_{\rm eff} > 25.0$ mag arcsec^{-2}.

7 CONCLUSIONS

In this paper we used a deep, wide-field CCD imaging survey, the MGC (Liske et al. 2003), to test the photometric accuracy and completeness of the 2dFGRS and SDSS-EDR, as well as the photometric accuracy of SCOS and SDSS-DR1. The main photometric and completeness results for the 2dFGRS and SDSS are summarized in Tables 2 , 3, 4, 6 and 7. The comparison between the MGC and SDSS-DR1 finds that $\Delta m = 0.039 \pm 0.005$ mag with a scatter of 0.086 mag per galaxy. The stellar catalogue has photometry with $\Delta m = 0.044 \pm 0.005$ mag with a scatter of 0.046 mag, once the difference between Kron and Petrosian magnitudes and the field-to-field scatter has been taken into account. The field-to-field scatter in the MGC is ∼0.035 mag. We estimate that the 'galaxy measurement' error, a combination of decreasing signal-to-noise ratio per pixel and the difference between Kron and Petrosian magnitudes, contributes to a scatter of 0.06 mag in the galaxy errors. There is a small scale error of 2.7 per cent for bright galaxies, but faint galaxies and stars have extremely small scale errors of ∼0.5 per cent compared with the MGC. However, the fluxes of LSBGs $\mu_{\rm eff} > 24.5$ mag arcsec^{-2} are systematically underestimated by ∼0.1 mag.

The SDSS-EDR has similar scale errors and errors with surface brightness to SDSS-DR1. The significant differences are an offset of 0.007 mag, with the SDSS-DR1 magnitudes slightly brighter, and also a reduced standard deviation per galaxy for the SDSS-DR1.

Since the 2dFGRS and SCOS magnitudes in the 2dFGRS data base have been calibrated using SDSS-EDR photometry, the offset with respect to the MGC should be the same, and indeed it is within

the expected errors. Of the four data sets compared to the MGC, the 2dFGRS has the worst photometry, with $B_{\rm MGC} - B_{\rm 2dF} = (0.035 \pm 0.005)$ mag with a scatter of 0.142 mag per galaxy and a very large scale error, 5.7 per cent, which probably comes from non-linearities in the photometric plates causing the flux of high surface brightness objects to be significantly underestimated (see Fig. 7). High surface brightness objects have their fluxes underestimated in the 2dFGRS by $\sim$0.18 mag.

The SCOS magnitudes are a significant improvement on the 2dFGRS magnitudes, with a lower variance and especially with regard to the variation in Δm with surface brightness. This results in a reduced scale error and the SCOS photometry is well matched to the SDSS-EDR. However, while the scale error compared to the MGC is lower than the 2dFGRS scale error, it is still quite large (4.5 per cent). Both the SCOS and SDSS-DR1 show significant improvements when compared to the 2dFDRS and SDSS-EDR, respectively, as expected with later releases.

The main source of error in the comparison of the offsets is the colour equations used to compare the photometry. These need to be accurate to $<$0.002 mag before random errors become the main source of error in the comparison between 2dFGRS and MGC.

While it is impossible to say for certain which survey has the best photometry, as all the checks are relative, some trends can be seen. The MGC seems to be fainter by 0.04 mag than all the other surveys, but since the 2dFGRS and SCOS are matched to the SDSS-EDR, we have to be very careful on this matter. The scale error results cannot be interpreted in an absolute sense either. However, the standard deviation per galaxy can be a useful indicator. It is lowest between the MGC and DR1 (apart from between the EDR and DR1, which are taken from the same data), indicating that these are the two best surveys. It is difficult to tell if the MGC or the DR1 is the best, since the MGC has the lowest standard deviation compared to the APM, but DR1 has the lowest compared to SCOS.

We find that (5.2 ± 0.3) per cent of the objects classified as galaxies in the 2dFGRS are stars, (7.0 ± 0.4) per cent are multiple objects and (0.9 ± 0.1) per cent are artefacts. When compared to the MGC galaxy catalogue, we find that the 2dFGRS is incomplete by (8.7 ± 0.6) per cent by $B_{\rm MGC} = 19.0$ mag. Since the spectroscopic data show that (5.6 ± 1.3) per cent of the MGC galaxy catalogue are misclassified as stars, then we conclude that (14.3 ± 1.4) per cent of galaxies are missing from the 2dFGRS brighter than $B_{\rm MGC} = 19.0$ mag.

The missing galaxies that are seen in the MGC galaxy catalogue can be split into four classes: LSBGs, (6 ± 2) per cent; unresolved objects, (18 ± 3) per cent; blended objects, (53 ± 5) per cent; and normal galaxies, (19 ± 3) per cent. This is in line with the findings of Pimbblet et al. (2001).

In the SDSS-EDR, there is (1.3 ± 0.1) per cent stellar contamination, (5.3 ± 1.0) per cent galaxies are misclassified as stars and (0.45 ± 0.07) per cent are artefacts. The SDSS-EDR galaxy catalogue is incomplete by (1.8 ± 0.1) per cent, so (7.1 ± 1.0) per cent of galaxies brighter than $B_{\rm MGC} = 20.0$ mag are missing from the SDSS-EDR. The fraction of QSOs in the stellar catalogues of the MGC and SDSS-EDR is (2.1 ± 0.4) per cent.

The true impact of any incompleteness on measurements of the luminosity function can only be known with assurance by constructing a high and uniformly complete redshift survey. We have found that even modern CCD surveys such as the MGC and SDSS-EDR are missing 5–7 per cent of the galaxy sample due to difficulties in star–galaxy separation. This means that number counts and luminosity functions will have to be revised upwards, and the shapes may have to be revised if the redshift distribution of these objects does not follow the redshift distribution of the known galaxy population. Since these galaxies are hard to separate from stars, they are likely to be compact galaxies, possibly from the same population as found by Drinkwater (1999) in Fornax. They estimated that (3.2 ± 1.2) per cent of compact galaxies were missed from 2dFGRS. This is compatible with our value of (5.6 ± 1.3) per cent, given that the Fornax cluster at $z = 0.0046$ is significantly closer than the average galaxy in our sample ($z = 0.1$). At the distance to Fornax, fewer galaxies should be unresolved since they would have to have scalelengths $R < 100$ pc. The constraints on the galaxies in our sample are $R < 2$ kpc on average, with a final fraction (1.4 ± 1.3) per cent of our galaxy sample in the same range as the Fornax cluster members. Since all these scalelengths are upper limits, it is impossible to say for certain whether these constitute the same types of galaxy. These objects will be analysed in more detail in a later paper.

ACKNOWLEDGMENTS

We would like to thank Keith Horne and Mike Merrifield for their comments on NJGC's thesis, which led to improvements in this paper. The MGC data were obtained through the Isaac Newton Group's Wide Field Camera Survey Programme. The Isaac Newton Telescope is operated on the island of La Palma by the Isaac Newton Group in the Spanish Observatorio del Roque de los Muchachos of the Instituto de Astrofisica de Canarias. We also thank CASU for their data reduction and astrometric calibration.

Funding for the creation and distribution of the SDSS Archive has been provided by the Alfred P. Sloan Foundation, the Participating Institutions, the National Aeronautics and Space Administration, the National Science Foundation, the US Department of Energy, the Japanese Monbukagakusho, and the Max Planck Society. The SDSS is managed by the Astrophysical Research Consortium (ARC) for the Participating Institutions. The Participating Institutions are the University of Chicago, Fermilab, the Institute for Advanced Study, the Japan Participation Group, Johns Hopkins University, Los Alamos National Laboratory, the Max-Planck-Institute for Astronomy (MPIA), the Max-Planck-Institute for Astrophysics (MPA), New Mexico State University, University of Pittsburgh, Princeton University, the United States Naval Observatory, and the University of Washington.

The 2dFGRS data were obtained via the two-degree facility on the 3.9-m Anglo-Australian Observatory. We would like to thank Bruce Peterson for help in accessing the 2dFGRS data base and Ivan Baldry for his useful comments on SDSS photometry. We thank all those involved in the smooth running and continued success of the 2dF and the AAO. NJGC and DJL were funded by PPARC research studentships during the course of this work.

REFERENCES

Abazajian K. et al., 2003, AJ, 126, 2081
Arnouts S., Vandame B., Benoist C., Groenewegen M. A. T., da Costa L., Schirmer M., Mignani R. P., Slijkhuis R., 2001, A&A, 379, 740
Baldry I. K. et al., 2002, ApJ, 569, 582
Bertin E., Arnouts S., 1996, A&AS, 117, 393
Blair M., Gilmore G., 1982, PASP, 94, 42
Blanton M. R. et al., 2001, AJ, 121, 2358
Blanton M. R. et al., 2003, ApJ, 592, 819
Cole S. et al., 2001, MNRAS, 326, 255
Colless M. M. et al., 2001, MNRAS, 328, 1039
Colless M. M. et al., 2003, The 2dF Galaxy Survey: The Final Data Release (astro-ph/0306581)
Cross N. J. G., 2002, PhD thesis, Univ. St Andrews

Cross N. J. G., Driver S. P., 2002, MNRAS, 329, 579
Cross N. J. G. et al., 2001, MNRAS, 324, 825
de Propris R. et al., 2003, MNRAS, 342, 725
Disney M., 1976, Nat, 263, 573
Drinkwater M. J., 1999, ApJ, 511, L97
Efstathiou G. et al., 2002, MNRAS, 330, L29
Elgaroy O. et al., 2002, Phys. Rev. Lett., 89, 1301
Folkes S. et al., 1999, MNRAS, 308, 459
Francis P. J., Nelson B., Cutri R., 2004, AJ, in press (astro-ph/0310396)
Fukugita M., Ichikawa T., Gunn J. E., Doi M., Shimasaku K., Schneider D. P., 1996, AJ, 111, 1748
Hambly N. C. et al., 2001, MNRAS, 326, 1279
Impey C., Bothun G., 1997, ARA&A, 35, 267
Impey C. D., Sprayberry D., Irwin M. J., Bothun G. D., 1996, ApJS, 105, 209
Jarrett T. H., Chester T., Cutri R., Schneider S., Skrutskie M., Huchra J. P., 2000, AJ, 119, 2498
Kron R. G., 1980, ApJS, 43, 305
Lemon D. J., 2003, PhD thesis, Univ. St Andrews
Lewis I. J. et al., 2002, MNRAS, 334, 673
Liske J., Lemon D. J., Driver S. P., Cross N. J. G., Couch W. J., 2003, MNRAS, 344, 307 (MGC1)
Maddox S. J., Sutherland W. J., Efstathiou G., Loveday J., 1990a, MNRAS, 243, 692
Maddox S. J., Efstathiou G., Sutherland W. J., 1990b, MNRAS, 246, 433
Madgwick D. S. et al., 2002, MNRAS, 333, 133
Norberg P. et al., 2001, MNRAS, 328, 64
Norberg P. et al., 2002a, MNRAS, 332, 827
Norberg P. et al., 2002b, MNRAS, 336, 907
O'Neil K., Bothun G. D., 2000, ApJ, 529, 811
Peacock J. A. et al., 2001, Nat, 410, 169
Pimbblet K. A., Smail I., Edge A. C., Couch W. J., O'Hely E., Zabludoff A. I., 2001, MNRAS, 327, 588
Raychaudhury S., Lynden-Bell D., Scharf C., Hudson M. J., 1994, BAAS, 184, 3806
Schlegel D., Finkbeiner D. P., Davis M., 1998, ApJ, 500, 525
Smith J. A. et al., 2002, AJ, 123, 2121
Sprayberry D., Impey C. D., Irwin M. J., Bothun G. D., 1997, ApJ, 482, 104
Stoughton C. et al., 2002, AJ, 123, 485
Verde L. et al., 2002, MNRAS, 335, 432
Yasuda N. et al., 2001, ApJ, 122, 1104
York D. G. et al., 2000, AJ, 120, 1579

APPENDIX A: COLOUR EQUATIONS

Since the present paper is concerned with a high-precision comparison of photometry, it is necessary to take particular care with the colour equations that relate different systems.

A1 MGC

The calibration of the MGC was performed relative to Landolt standards, which use the Johnson–Cousins system. The empirical colour equation (with an imposed Vega zero-point) is

$$B_{\rm MGC} = B - 0.145(B - V). \tag{A1}$$

A2 SDSS

Here, it is necessary to distinguish clearly between (at least) four systems:

(i) USNO (u' g' r' i' z'),
(ii) EDR (u^* g^* r^* i^* z^*),
(iii) DR1 (*ugriz*),
(iv) AB ($u_{\rm AB} g_{\rm AB} r_{\rm AB} i_{\rm AB} z_{\rm AB}$).

The last of these is intended to denote the ultimate SDSS system of *AB* magnitudes, with the philosophy described by Fukugita et al. (1996) – but reflecting the fact that the filters used in reality on the SDSS 2.5-m differ slightly from the responses assumed by Fukugita et al. The 2.5-m filters also differ significantly from the filters used by the USNO to define the network of SDSS standard stars (Smith et al. 2002). The necessary colour equations for the transformation may be found online.[5]

Here, we are mainly concerned with the cases of g and r, for which

$$g = g' + 0.060[(g' - r') - 0.53], \tag{A2}$$

$$r = r' + 0.035[(r' - i') - 0.21]. \tag{A3}$$

An unfortunate aspect of this transformation is that the colour equation for r involves i magnitudes. However, the offset $r - r'$ also correlates well with $g - r$, and the following equation was obtained, which allows us to work entirely within (g, r) space:

$$r = r' + 0.016[(g' - r') - 0.53]. \tag{A4}$$

Using these corrections, the conversions to *BVR* given by Smith et al. (2002) can be cast in terms of DR1 magnitudes:

$$B = g + 0.39(g - r) + 0.21, \tag{A5}$$

$$V = g - 0.58(g - r) - 0.01, \tag{A6}$$

$$R = r - 0.15(g - r) - 0.14. \tag{A7}$$

These empirical relations are very similar to the equations given by Fukugita et al. (1996):

$$B = g_{\rm AB} + 0.42(g_{\rm AB} - r_{\rm AB}) + 0.20, \tag{A8}$$

$$V = g_{\rm AB} - 0.53(g_{\rm AB} - r_{\rm AB}) + 0.00, \tag{A9}$$

$$R = r_{\rm AB} - 0.09(g_{\rm AB} - r_{\rm AB}) - 0.16. \tag{A10}$$

Finally, there is the issue that the current SDSS magnitudes are not yet believed to be zero-pointed to a perfect AB system. Blanton et al. (2003) give the following mean corrections, in order to obtain true *AB* magnitudes from the EDR data:

$$g_{\rm AB} = g^* + 0.036, \tag{A11}$$

$$r_{\rm AB} = r^* + 0.015. \tag{A12}$$

The difference between the DR1 magnitudes and EDR magnitudes does not include the correction to *AB* magnitudes. The difference only involves the Smith et al. (2002) updates to the Fukugita et al. (1996) standard star system and the improvements to the photometric pipeline detailed in Abazajian et al. (2002). These changes are expected to produce a smaller offset than the corrections to *AB* magnitudes.

[5] http://www.sdss.org/dr1/algorithms/jeg_photometric_eq_dr1.html

A3 2dFGRS

The final calibration of the 2dFGRS for the public data release involved recalibration of the SuperCosmos photometry, using a zero-point that was based largely on SDSS-EDR data, but with the Blanton et al. (2003) conversion to *AB*. The Fukugita et al. (1996) colour equations were assumed, and SCOS magnitudes were given a Vega zero-point, with the following empirical colour equations:

$$b_{\rm J} = B - 0.30(B - V), \tag{A13}$$

$$r_{\rm F} = R + 0.16(V - R). \tag{A14}$$

Explicitly, the relations used in terms of EDR magnitudes were:

$$b_{\rm J} = g^* + 0.130(g^* - r^*) + 0.189, \tag{A15}$$

$$r_{\rm F} = r^* - 0.115. \tag{A16}$$

If we were to adopt the empirical conversion between *gr* and *BVR* given earlier, and ignore any small differences between EDR and DR1, these differences would now imply

$$b_{\rm J} = B - 0.27(B - V) + 0.00, \tag{A17}$$

$$r_{\rm F} = R + 0.26(V - R) - 0.03. \tag{A18}$$

We thus see that the 2dFGRS $b_{\rm J}$ magnitudes are very accurately on a Vega system, and need no adjusting. Arguably the $r_{\rm F}$ magnitudes are too bright for a Vega zero-point by 0.03 mag.; this is comparable to the overall zero-point uncertainty, and in any case we are not concerned with the $r_{\rm F}$ magnitudes in this paper.

A4 Predictions from the EDR

In practice, we will wish to predict $B_{\rm MGC}$ and $b_{\rm J}$ magnitudes from the SDSS photometry. We will ignore the small differences between the EDR and DR1, and use the above relations between $B_{\rm MGC}$ and $b_{\rm 2dF}$ and (B, V), relating *gr* to *BV* as in the revised empirical relations from Smith et al. (2002). This yields

$$B_{\rm MGC} = g + 0.25(g - r) + 0.18 \tag{A19}$$

(or the identical estimator, in the case where EDR g^*r^* magnitudes are used). For the 2dFGRS, we of course retain the colour equation used in calibration:

$$b_{\rm 2dF} = g + 0.13(g - r) + 0.19. \tag{A20}$$

Finally, we can eliminate SDSS data from these definitions, so that MGC magnitudes can be predicted from SCOS data alone:

$$B_{\rm MGC} = b_{\rm SCOS} + 0.11(b_{\rm SCOS} - r_{\rm SCOS}) - 0.04. \tag{A21}$$

One important final point remains to be made. The colour equations above match the MGC to the SDSS-DR1 and EDR *ugriz*, $u^*g^*r^*i^*z^*$ directly, not to the AB system, so using the Blanton et al. (2003) corrections to *AB* later is incorrect. The colour equations convert the *ugriz* to $B_{\rm MGC}$ whether the SDSS magnitudes are on the standard AB system or not, since the colour equations were calculated for the *ugriz* filters, not the $u_{\rm AB}g_{\rm AB}r_{\rm AB}i_{\rm AB}z_{\rm AB}$ filters.

This paper has been typeset from a TEX/LATEX file prepared by the author.